THE PREDICTION OF AERODYNAMIC FORCE AND MOMENT COEFFICIENTS ON ELLIPTIC CONE BODIES AT BOTH ANGLE OF ATTACK AND SIDESLIP BY USE OF NEWTONIAN IMPACT THEORY

by

William R. Wells

Thesis submitted to the Graduate Faculty of the

Virginia Polytechnic Institute

in candidacy for the degree of

MASTER OF SCIENCE

in

AERONAUTICAL ENGINEERING

May 1961

Blacksburg, Virginia

II. TABLE OF CONTENTS

III. LIST OF FIGURES

FIGURE PAGE

IV. SYMBOLS

A	reference area
a	$\cos \alpha \cos \beta$
B	reference length
b	body width at base of unsegmented cone
C_A	axial force coefficient, $\frac{F_X}{q_\infty A}$
C_D	drag coefficient, $\frac{F_D}{q_\infty A}$
C_L	lift coefficient, $\frac{F_L}{q_\infty A}$
C_l	rolling-moment coefficient, taken about center line of unsegmented cone, $\frac{M_X}{qAB}$
C_{l_β}	$\frac{\partial C_l}{\partial \beta}$, per degree
$C_{L,max}$	maximum lift coefficient
C_m	pitching-moment coefficient, $\frac{M_Y}{q_\infty AB}$
C_{m_α}	$\frac{\partial C_m}{\partial \alpha}$, per degree
C_N	normal force coefficient, $\frac{F_Z}{q_\infty A}$
C_n	yawing moment coefficient, $\frac{M_Z}{q_\infty AB}$
C_{N_α}	$\frac{\partial C_N}{\partial \alpha}$, per degree
C_{n_β}	$\frac{\partial C_n}{\partial \beta}$, per degree
C_P	pressure coefficient, $\frac{P - P_\infty}{q_\infty}$

C_Y	side-force coefficient, $\frac{F_Y}{q_\infty A}$
C_{Y_β}	$\frac{\partial C_Y}{\partial \beta}$, per degree
c	$-\sin \beta$
d	$\sin \alpha \cos \beta$
F_D	drag force
F_L	lift force
F_X	axial force in direction of X axis
F_Y	side force in direction of Y axis
F_Z	normal force in direction of Z axis
f(x,y,z)	equation of general surface
$\vec{i},\vec{j},\vec{k}$	unit vectors in direction of X, Y, and Z axes, respectively
k	$\frac{\sin \theta_{xz}}{\sin \theta_{xy}}$
L	length of cone
M	Mach number
m	$\frac{\tan \theta_{xz}}{\tan \theta_{xy}}$
M_X	moment about X axis
M_Y	moment about Y axis
M_Z	moment about Z axis
$\vec{n}$	unit vector normal to surface
p	local pressure
p_∞	free-stream pressure
q_∞	free-stream dynamic pressure
R	base radius of circular cone
$\vec{V}$	unit free-stream wind vector

X,Y,Z	rectangular Cartesian coordinate axes
x,y,z	rectangular Cartesian coordinates
x,ρ,φ	cylindrical polar coordinates
α	angle of attack
β	angle of sideslip
δ	$1 - k^2$
η	angle between unit surface normal and wind vectors
θ	circular cone semiapex angle
θ_{xy}	elliptical cone semiapex angle in the horizontal direction
θ_{xz}	elliptical cone semiapex angle in the vertical direction
φ_1	upper limit of integration
φ_2	lower limit of integration
Ψ	$1 + (m^2 - 1) \sin^2\varphi$
Ω	$1 + (m^2k^2 - 1) \sin^2\varphi$

V. INTRODUCTION

Newtonian impact theory, in recent years, has proven to be one of the more useful theories for the prediction of aerodynamic forces and moments on bodies in the hypersonic flow regimes ($5 < M < \infty$). This theory predicts the pressure coefficient, for the part of the body exposed to the flow, to be given by twice the square of the cosine of the angle between the free-stream velocity vector and the normal vector to the body surface. It does not, however, specify the pressures on surfaces that are in the expansion region or "shadowed" region. For high speeds it is usually assumed that the pressure coefficient is zero in this region. The force and moment coefficients are obtained by integrating the incremental forces acting on the body over the part exposed to the flow.

Current interest in vehicles capable of reentry has indicated a definite need for closed expressions for the aerodynamic coefficients, obtained by Newtonian impact theory, of both elliptical and circular cone bodies.

A theoretical treatment of the full circular cone at angles of attack in Newtonian flow was performed in reference 1. This analysis was followed by reference 2 in which the full oblate elliptical cone at angles of attack was treated. A great deal of experimental work on the cones at hypersonic speeds followed the work mentioned above. Comparisons of experiment and Newtonian theory on the cones have been made in references 4, 5, 6, and 8.

This analysis intends to extend the above applications of the theory to the case of segments of these elliptical cones at both angles of attack and sideslip. The prolate as well as the oblate elliptical cone is

treated, and the circular cone segments are obtained as a special case of the general results.

Comparisons are made with available experimental results to provide some indication of the usefulness of this theory in the prediction of the aerodynamic coefficients. These comparisons include variations in some of the longitudinal characteristics and stability derivatives with change in angle of attack, cone half angle and body cross section. These experimental results were obtained at Mach numbers of 6.8 and 9.6 and are discussed in more detail in references 4 and 8.

VI. ANALYSIS

A. Development of General Expressions for the Elliptic Conic Segment

Newtonian impact theory predicts the pressure coefficient for the part of the body exposed to the flow to be given by twice the cosine squared of the included angle between the normal to the body and the wind vectors (that is, $C_p = 2\cos^2\eta$). The angle, η, is found by taking the dot product of the normalized wind and surface gradient vectors. If $f(x,y,z) = 0$ is the equation of a general surface, then the surface gradient of this surface is

$$\nabla f = \frac{\partial f}{\partial x}\vec{i} + \frac{\partial f}{\partial y}\vec{j} + \frac{\partial f}{\partial z}\vec{k} \tag{1}$$

and the unit normal vector is

$$\vec{n} = \frac{\nabla f}{|\nabla f|} = \frac{\frac{\partial f}{\partial x}\vec{i} + \frac{\partial f}{\partial y}\vec{j} + \frac{\partial f}{\partial z}\vec{k}}{\sqrt{\left(\frac{\partial f}{\partial x}\right)^2 + \left(\frac{\partial f}{\partial y}\right)^2 + \left(\frac{\partial f}{\partial z}\right)^2}} \tag{2}$$

The coordinate system for a general body is shown in figure 1.

The normalized wind vector, $\vec{V}$, for a body inclined to the flow at both angles of attack and sideslip, is given as

$$\vec{V} = -\cos\alpha\cos\beta\,\vec{i} + \sin\beta\,\vec{j} + \sin\alpha\cos\beta\,\vec{k} \tag{3}$$

The wind vector and its components are also shown in figure 1.

The pressure coefficient, C_p, is then written as

$$C_p = 2(\vec{n} \cdot \vec{V})^2 \tag{4}$$

When only pressure forces are considered, the general force coefficient is given as

$$C_F = \frac{F}{q_\infty S} = \frac{1}{S} \int_{S_F} \left(\frac{p - p_\infty}{q_\infty} \right) dS_F = \frac{1}{S} \int_{S_F} C_p \, dS_F \tag{5}$$

In the above expression, S is a reference area and S_F is the projected area over which the pressure coefficient, C_p, is defined.

The moment coefficient is similarly given as

$$C_m = \frac{1}{SR} \int_{S_F} rC_p \, dS_F \tag{6}$$

where r is the moment arm and R is a reference length.

It is necessary to determine the part of the body that is shielded from the flow, since it will be assumed that the pressure on that part of the body has the free-stream value. This shadowed or shielded region is shown as the shaded region on the body in figure 1. The curve BAC, formed by the winds tangency to the surface, outlines the shadowed region on the surface f. The equation of this curve is given by the condition that

$$\cos \eta = 0 \tag{7}$$

The analysis will be concerned with obtaining closed form expressions for equations (5) and (6) for the special case of an elliptical cone segment at angles of attack and sideslip.

The equation of the surface of an elliptic cone can be written as

$$f(x,y,z) = 0 = -x^2 + \left(\frac{2L}{b}\right)^2 y^2 + \left(\frac{2L}{t}\right)^2 z^2 \tag{8}$$

where b, t, and L are the maximum thickness, width, and length, respectively, of the elliptic cone body. Another convenient form of this equation can be obtained by use of the angles, θ_{xy} and θ_{xz}, shown in figure 2 and defined to be the cone half angles in the x-y and x-z plenes, respectively. This equation is

$$f(x,y,z) = 0 = -x^2 + \frac{y^2}{\tan^2\theta_{xy}} + \frac{z^2}{\tan^2\theta_{xz}} \tag{9}$$

The analysis will, for convenience, be done using this notation but the final expressions will be written with the physical characteristics, t, b, and L contained in them. The ratios, $\frac{t}{b}$, and $\frac{t}{b}\sqrt{\frac{b^2 + 4L^2}{t^2 + 4L^2}}$ will be defined, for convenience, to be m and k, respectively. m and k are also seen to be simply $\frac{\tan\theta_{xz}}{\tan\theta_{xy}}$ and $\frac{\sin\theta_{xz}}{\sin\theta_{xy}}$, respectively. The above definitions of m and k reveal that if $m \geq 1$ so is $k \geq 1$ or if $m \leq 1$ so is $k \leq 1$. It is also seen that a value of $m < 1$ reveals that the ellipse is one such that its major axis is in the width direction and minor axes in the thickness direction. Similarly for $m > 1$, the ellipse is such that the major axes are in the thickness direction and minor axes in width direction. A value of $m = 1$ corresponds to a circular cone whose major and minor axes are equal. These three cases are shown in figure 3.

A convenient manner in which to choose arbitrary segments of this conic body is through the assignment of definite values of the angles,

φ, defined in figure 2. In this figure, φ is seen to be zero at upper vertical and increase positively in the counterclockwise direction. For this reason the Cartesian coordinates (x,y,z) will be replaced by cylindrical polar coordinates (x,φ,ρ). The transformation is

$$\left.\begin{aligned} x &= x \\ y &= \rho \sin \varphi \\ z &= \rho \cos \varphi \end{aligned}\right\} \tag{10}$$

The surface gradient vector is

$$\nabla f = -2x\,\vec{i} + 2y \cot^2\theta_{xy}\,\vec{j} - 2z \cot^2\theta_{xz}\,\vec{k} \tag{11}$$

The unit normal is

$$\vec{n} = \frac{x\,\vec{i} - y \cot^2\theta_{xz}\,\vec{j} - z \cot^2\theta_{xz}\,\vec{k}}{\sqrt{x^2 + y^2\cot^4\theta_{xy} + z^2\cot^4\theta_{xz}}} \tag{12}$$

At the surface $f = 0$, this gives the following relation between x, ρ, and φ:

$$x = -\rho \sqrt{\sin^2\varphi \cot^2\theta_{xy} + \cos^2\varphi \cot^2\theta_{xz}} \tag{13}$$

Then in terms of ρ and φ, the unit normal becomes

$$\vec{n} = \frac{-\sin\theta_{xz}\sqrt{m^2\sin^2\varphi + \cos^2\varphi}\,\vec{i} - mk \cos\theta_{xy} \sin\varphi\,\vec{j} - \cos\theta_{xz}\cos\varphi\,\vec{k}}{\sqrt{m^2k^2\sin^2\varphi + \cos^2\varphi}} \tag{14}$$

The dot product of expressions (3) and (14) gives

$$\cos \eta = \frac{1}{\sqrt{m^2k^2\sin^2\varphi + \cos^2\varphi}}\Big[\cos \alpha \cos \beta \sin \theta_{xz} \sqrt{m^2\sin^2\varphi + \cos^2\varphi}$$

$$-mk \sin \beta \cos \theta_{xy} \sin \varphi - \sin \alpha \cos \beta \cos \theta_{xz} \cos \varphi\Big] \tag{15}$$

If the following definitions are made,

$$\left.\begin{aligned} a &= \cos \alpha \cos \beta \\ c &= -\sin \beta \\ d &= \sin \alpha \cos \beta \end{aligned}\right\} \tag{16}$$

then the pressure coefficient, C_p, is

$$C_p = \frac{2}{(m^2k^2\sin^2\varphi + \cos^2\varphi)}\Big(a \sin \theta_{xz} \sqrt{m^2\sin^2\varphi + \cos^2\varphi}$$

$$+ mkc \cos \theta_{xy} \sin \varphi - d \cos \theta_{xz} \cos \varphi\Big)^2 \tag{17}$$

The shadowed region on the surface can now be conveniently determined by letting equation (17) be zero. This gives the following expression for φ which is the variation of φ along the shadow plane

$$\varphi = \cot^{-1}\left[\frac{k^2cd \cos^2\theta_{xy} \pm am \sin \theta_{xz} \sqrt{k^2c^2\cos^2\theta_{xy} + \left(d^2\cos^2\theta_{xz} - a^2\sin^2\theta_{xz}\right)}}{d^2\cos^2\theta_{xz} - a^2\sin^2\theta_{xz}}\right] \tag{18}$$

The plus and minus sign appearing in the above expression indicates two values of φ for each angle of attack and conic body. Physically, this means that one sign is to be taken to give the value of φ, φ_1, at which shadow begins and the second sign is to be used with the value of φ, φ_2, at which shadow ends. The following sketch will serve to illustrate the manner in which the signs are to be taken for φ_1 and φ_2.

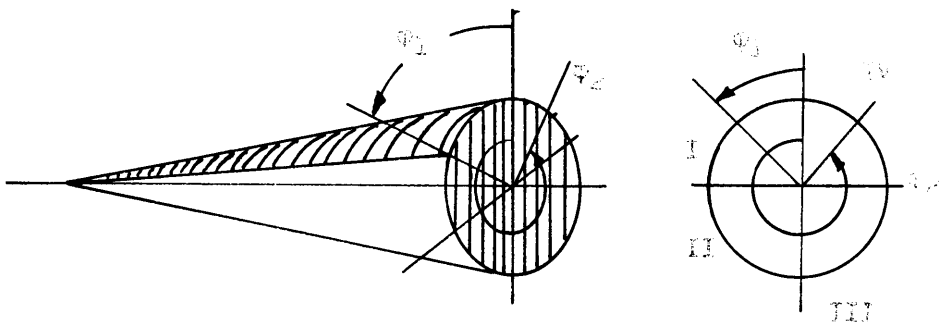

Sketch 1.

The sign that goes with φ_1 can be determined as follows: first, it can be seen that for positive values of β (that is, the wind approaching the body from the right) the point φ_1 must fall in either the first or second quadrant. Similarly φ_2 must be in either the first or fourth quadrant since the curved surface associated with the third quadrant is always exposed to the wind. Then for positive values of β, $0 \leq \varphi_1 \leq \pi$ and $-\pi/2 \leq \varphi_2 \leq \pi/2$. Then for $\beta = 0$

$$\varphi = \cot^{-1}\left[\pm \frac{am \sin \theta_{xz}}{\sqrt{d^2\cos^2\theta_{xz} - a^2\sin^2\theta_{xz}}}\right] \qquad (19)$$

Thus it is seen that the positive sign is taken for φ_1 and the negative for φ_2. Then

$$\varphi_1 = \cot^{-1}\left[\frac{k^2cd\cos^2\theta_{xy} + am\sin\theta_{xz}\sqrt{k^2c^2\cos^2\theta_{xy} + d^2\cos^2\theta_{xz} - a^2\sin^2\theta_{xz}}}{d^2\cos^2\theta_{xz} - a^2\sin^2\theta_{xz}}\right] \tag{20}$$

$$\varphi_2 = \cot^{-1}\left[\frac{k^2cd\cos^2\theta_{xz} - am\sin\theta_{xz}\sqrt{k^2c^2\cos^2\theta_{xy} + d^2\cos^2\theta_{xz} - a^2\sin^2\theta_{xz}}}{d^2\cos^2\theta_{xz} - a^2\sin^2\theta_{xz}}\right] \tag{21}$$

These expressions give a simple and quick test to determine what angles of attack cause shadow to exist. For the above angles to exist physically, the quantity under the radical must be positive. Therefore, for

$$k^2c^2\cos^2\theta_{xy} + d^2\cos^2\theta_{xz} - a^2\sin^2\theta_{xz} > 0$$

shadow exists. For

$$k^2c^2\cos^2\theta_{xy} + d^2\cos^2\theta_{xz} - a^2\sin^2\theta_{xz} < 0$$

shadow does not occur on the body. For

$$k^2c^2\cos^2\theta_{xy} + d^2\cos^2\theta_{xz} - a^2\sin^2\theta_{xz} = 0$$

then shadow exists if either β or α are not zero. If shadow does exist, it is necessary to compute φ_1 and φ_2 from equations (20) and (21)

and compare these with the values of φ_1 and φ_2 imposed by the body limits.

The aerodynamic coefficients, C_N, C_A, C_Y, C_m, C_n, and C_l can be obtained by integration of equation (5) with the expression for C_p in equation (17) substituted into it.

It is also necessary to determine the elements of area, dS_N, dS_A, and dS_Y in terms of the coordinates (x,φ,ρ). The area elements are

$$dS_N = dx\,dy = \begin{vmatrix} \frac{\partial x}{\partial x} & \frac{\partial x}{\partial \varphi} \\ \frac{\partial y}{\partial x} & \frac{\partial y}{\partial \varphi} \end{vmatrix} dx\,d\varphi = \frac{-x \tan \theta_{xz} \cos \varphi \, dx\,d\varphi}{(m^2\sin^2\varphi + \cos^2\varphi)^{3/2}} \tag{22}$$

$$dS_Y = dx\,dz = \begin{vmatrix} \frac{\partial x}{\partial x} & \frac{\partial x}{\partial \varphi} \\ \frac{\partial z}{\partial x} & \frac{\partial z}{\partial \varphi} \end{vmatrix} dx\,d\varphi = \frac{xm^2 \tan \theta_{xz} \sin \varphi \, dx\,d\varphi}{(m^2\sin^2\varphi + \cos^2\varphi)^{3/2}} \tag{23}$$

and

$$dS_A = dy\,dz = \begin{vmatrix} \frac{\partial y}{\partial \varphi} & \frac{\partial y}{\partial \rho} \\ \frac{\partial z}{\partial \varphi} & \frac{\partial z}{\partial \rho} \end{vmatrix} d\rho\,d\varphi = \rho\,d\rho\,d\varphi \tag{24}$$

The force coefficients are then written

$$C_N = \frac{1}{A} \int_{x_1}^{x_2} \int_{\varphi_1}^{\varphi_2} \frac{-C_p\, x \tan \theta_{xz} \cos \varphi \, dx\,d\varphi}{(m^2\sin^2\varphi + \cos^2\varphi)^{3/2}} \tag{25}$$

$$C_A = \frac{1}{A} \int_{\rho_1}^{\rho_2} \int_{\varphi_1}^{\varphi_2} C_p \, \rho \, d\rho \, d\varphi \tag{26}$$

$$C_Y = \frac{1}{A} \int_{x_1}^{x_2} \int_{\varphi_1}^{\varphi_2} \frac{C_p \, x \tan \theta_{xz} \, m^2 \sin \varphi \, dx \, d\varphi}{(m^2 \sin^2\varphi + \cos^2\varphi)^{3/2}} \tag{27}$$

If it is assumed that the body exists in the x-direction from $x_1 = 0$ to $x_2 = -L$ (a sharp cone), then the above expressions can be integrated in the x-direction to give

$$C_N = - \frac{L^2}{2A} \int_{\varphi_1}^{\varphi_2} \frac{C_p \tan \theta_{xz} \cos \varphi \, d\varphi}{(m^2 \sin^2\varphi + \cos^2\varphi)^{3/2}} \tag{28}$$

$$C_A = \frac{L^2}{2A} \int_{\varphi_1}^{\varphi_2} \frac{\tan^2\theta_{xz} \, C_p \, d\varphi}{(m^2 \sin \varphi + \cos \varphi)} \tag{29}$$

$$C_Y = \frac{L^2}{2A} \int_{\varphi_1}^{\varphi_2} \frac{C_p \, m^2 \tan \theta_{xz} \sin \varphi \, d\varphi}{(m^2 \sin^2\varphi + \cos^2\varphi)^{3/2}} \tag{30}$$

The pitching-moment coefficient C_m can be obtained by considering the moments of the normal and axial forces. Thus, if one chooses a point on the center line at the base

$$C_m = \frac{1}{AB}\left[\int_{\rho_1}^{\rho_2}\int_{\varphi_1}^{\varphi_2} \rho\, C_p \cos\varphi\, d\rho\, d\varphi + \int_{x_1}^{x_2}\int_{\varphi_1}^{\varphi_2} C_p\, x(L - x)m^2 \tan\theta_{xz} \cos\varphi\, dx\, d\varphi\right] \tag{31}$$

If the x integration is performed from $x_1 = 0$ to $x_2 = L$, then

$$C_m = \frac{-L^3}{6AB}(1 - 2\tan^2\theta_{xz}) \int_{\varphi_1}^{\varphi_2} \frac{C_p \tan\theta_{xz}\, m^2 \cos\varphi\, d\varphi}{(m^2\sin^2\varphi + \cos^2\varphi)^{3/2}}$$

Or since

$$C_N = -\frac{L^2}{2A} \int_{\varphi_1}^{\varphi_2} \frac{C_p \tan\theta_{xz}\, m^2 \cos\varphi\, d\varphi}{(m^2\sin^2\varphi + \cos^2\varphi)^{3/2}}$$

then

$$C_m = \frac{L}{3B}(1 - 2\tan^2\theta_{xz})C_N \tag{32}$$

Similarly

$$C_n = \frac{L}{3B}(1 - 2\tan^2\theta_{xy})C_Y \tag{33}$$

The rolling moment coefficient about the center line of the cone is

$$C_l = \frac{L^3}{3AB}(m^2 - 1) \int_{\varphi_1}^{\varphi_2} \frac{\tan^2\theta_{xz}\, C_p \sin\varphi \cos\varphi\, d\varphi}{(m^2\sin^2\varphi + \cos^2\varphi)^2} \tag{34}$$

For brevity, the following definitions are made:

$$\Psi \equiv 1 + (m^2 - 1)\sin^2\varphi \tag{35}$$

$$\Omega \equiv 1 + (m^2k^2 - 1)\sin^2\varphi \tag{36}$$

If the expression for C_p in equation (17) with the above definitions are substituted into equations (28), (29), (30), and (34), the following is obtained:

$$C_N = \frac{L^2}{2A}\sin^2\theta_{xz}\left[2a^2\tan\theta_{xz} \int_{\varphi_1}^{\varphi_2} \frac{\cos\varphi\, d\varphi}{\Omega\sqrt{\Psi}}\right.$$

$$+ 4acm^2 \int_{\varphi_1}^{\varphi_2} \frac{\sin\varphi\cos\varphi\, d\varphi}{\Omega\Psi} - 4ad \int_{\varphi_1}^{\varphi_2} \frac{\cos^2\varphi\, d\varphi}{\Omega\Psi}$$

$$- 4cdm^2\cot\theta_{xz} \int_{\varphi_1}^{\varphi_2} \frac{\sin\varphi\cos\varphi\, d\varphi}{\Omega\Psi^{3/2}} + 2c^2m^2\cot\theta_{xy} \int_{\varphi_1}^{\varphi_2} \frac{\cos\varphi\sin^2\varphi\, d\varphi}{\Omega\Psi^{3/2}}$$

$$\left. + 2d^2\cot\theta_{xz} \int_{\varphi_1}^{\varphi_2} \frac{\cos^3\varphi\, d\varphi}{\Omega\Psi^{3/2}}\right] \tag{37}$$

$$C_A = \frac{L^2 \tan^2\theta_{xz} \sin^2\theta_{xz}}{A}\left[a^2 \int_{\varphi_1}^{\varphi_2} \frac{d\varphi}{\Omega} + 2acm \cot\theta_{xy} \int_{\varphi_1}^{\varphi_2} \frac{\sin\varphi\, d\varphi}{\Omega\sqrt{\psi}}\right.$$

$$- 2ad \cot\theta_{xz} \int_{\varphi_1}^{\varphi_2} \frac{\cos\varphi\, d\varphi}{\Omega\sqrt{\psi}} - 2cd \cot^2\theta_{xy} \int_{\varphi_1}^{\varphi_2} \frac{\cos\varphi \sin\varphi\, d\varphi}{\Omega\psi}$$

$$\left. + c^2m^2\cot^2\theta_{xy} \int_{\varphi_1}^{\varphi_2} \frac{\sin^2\varphi\, d\varphi}{\Omega\psi} + d^2\cot^2\theta_{xz} \int_{\varphi_1}^{\varphi_2} \frac{\cos^2\varphi\, d\varphi}{\Omega\psi}\right] \qquad (38)$$

$$C_Y = \frac{Lm^2\sin^2\theta_{xz}}{A}\left[a^2\tan\theta_{xz} \int_{\varphi_1}^{\varphi_2} \frac{\sin\varphi\, d\varphi}{\Omega\sqrt{\psi}} + 2acm^2 \int_{\varphi_1}^{\varphi_2} \frac{\sin^2\varphi\, d\varphi}{\Omega\psi}\right.$$

$$- 2ad \int_{\varphi_1}^{\varphi_2} \frac{\cos\varphi \sin\varphi\, d\varphi}{\Omega\psi} - 2cdm^2\cot\theta_{xz} \int_{\varphi_1}^{\varphi_2} \frac{\cos\varphi \sin^2\varphi\, d\varphi}{\Omega\psi^{3/2}}$$

$$\left. + m^3\cot\theta_{xy} \int_{\varphi_1}^{\varphi_2} \frac{\sin^3\varphi\, d\varphi}{\Omega\psi^{3/2}} + d^2\cot\theta_{xz} \int_{\varphi_1}^{\varphi_2} \frac{\sin\varphi \cos^2\varphi\, d\varphi}{\Omega\psi^{3/2}}\right] \qquad (39)$$

$$C_l = (m^2 - 1)\sin\theta_{xz}\tan\theta_{xz} \frac{L^3}{3AB}\left[2a^2 \int_{\varphi_1}^{\varphi_2} \frac{\cos\varphi \sin\varphi\, d\varphi}{\Omega\psi}\right.$$

$$+ 4acm \cot\theta_{xy} \int_{\varphi_1}^{\varphi_2} \frac{\sin^2\varphi \cos\varphi\, d\varphi}{\Omega\psi^{3/2}} - 4ad \cot\theta_{xz} \int_{\varphi_1}^{\varphi_2} \frac{\sin\varphi \cos\varphi\, d\varphi}{\Omega\psi^{3/2}}$$

$$- 4cd \cot^2\theta_{xy} \int_{\varphi_1}^{\varphi_2} \frac{\cos\varphi \sin^2\varphi\, d\varphi}{\Omega\psi^2} + 2c^2m^2\cot^2\theta_{xy} \int_{\varphi_1}^{\varphi_2} \frac{\sin^3\varphi \cos\varphi\, d\varphi}{\Omega\psi}$$

$$\left. + 2d \cot\theta_{xz} \int_{\varphi_1}^{\varphi_2} \frac{\cos^2\varphi \sin\varphi\, d\varphi}{\Omega\psi^2}\right] \qquad (40)$$

If the integrals in the foregoing equations are for brevity, called I_1, I_2, . . . I_6, J_1, J_2, . . . J_6, L_1, L_2, . . . L_6, M_1, M_2, . . . M_6, then these expressions can be written as

$$C_N = -\frac{L^2\sin^2\theta_{xz}}{2A}\Big[2a^2\tan\theta_{xz}\, I_1 + 4acm^2 I_2 - 4adI_3 - 4cdm^2\cot\theta_{xz}\, I_4 + 2c^2m^2\cot\theta_{xz}\, I_5 + 2d^2\cot\theta_{xz}\, I_6\Big] \tag{41}$$

$$C_A = \frac{L^2\tan^2\theta_{xz}\,\sin^2\theta_{xz}}{A}\Big[a^2 J_1 + 2acm\cot\theta_{xy}\, J_2 - 2ad\cot\theta_{xz}\, J_3 - 2cd\cot^2\theta_{xy}\, J_4 + c^2m^2\cot^2\theta_{xy}\, J_5 + d^2\cot^2\theta_{xz}\, J_6\Big] \tag{42}$$

$$C_Y = m^2\sin^2\theta_{xz}\,\frac{L^2}{A}\Big[a^2\tan\theta_{xz}\, L_1 + 2acm^2 L_2 - 2ad\, L_3 - 2cdm^2\cot\theta_{xz}\, L_4 + m^3c^2\cot\theta_{xy}\, L_5 + d^2\cot\theta_{xz}\, L_6\Big] \tag{43}$$

$$C_l = (m^2 - 1)\sin^2\theta_{xz}\,\tan^2\theta_{xz}\,\frac{L^3}{3AB}\Big[2a^2 M_1 + 4acm\cot\theta_{xy}\, M_2 - 4ad\cot\theta_{xz}\, M_3 - 4cd\cot^2\theta_{xy}\, M_4 + 2c^2m^2\cot^2\theta_{xy}\, M_5 + 2d^2\cot^2\theta_{xz}\, M_6\Big] \tag{44}$$

The above integrals are tabulated in the appendix. Some of these integrals have different expressions depending on whether m is less than, equal to, or greater than unity. The coefficients then have different

representations according to whether the major axis of the ellipse lies along the horizontal or vertical axis.

B. General and Special Cases of the Static Stability Derivatives

The static stability derivatives C_{N_α}, C_{m_α}, C_{n_β}, and C_{l_β} can be obtained from the force coefficients simply by differentiation. The differentiation is somewhat simple for the case of no shadow, that is, $c^2\cot^2\theta_{xy} + d^2\cot^2\theta_{xz} < a^2$, since the variable φ appearing in the integrated expressions is not a function of α and β. For the case of shadow, however, φ is a function of α and β and hence differentiation is rather laborious. In this case, it is easier to get the derivatives directly from the plots of the force coefficients.

Then for the case of no shadow

$$C_{N_\alpha} = \frac{-2L^2\sin^2\theta_{xz}}{A}\Big[- ad \tan\theta_{xz}\, I_1 - dcm^2 I_2 - (a^2 - d^2) I_3 - cam^2\cot\theta_{xz}\, I_4 + ad \cot\theta_{xz}\, I_6\Big] \tag{45}$$

$$C_{Y_\beta} = m^2\sin^2\theta_{xz}\,\frac{L^2}{A}\Big[+ 2ac\cos\alpha\tan\theta_{xz}\, L_1 - 2\cos\alpha\, m^2(1 - 2c^2) L_2 - 2cd\cos\alpha\, L_3 + 2m^2\cot\theta_{xz}\sin\alpha(1 - 2c^2) L_4 - 2m^2c\cos\beta\cot\theta_{xy}\, L_5 + 2cd\sin\alpha\cot\theta_{xz}\, L_6\Big] \tag{46}$$

$$C_{l_\beta} = (m^2 - 1)\sin^2\theta_{xz} \tan^2\theta_{xz} \frac{L^3}{3AB}\Big[4ac \cos\alpha M_1 - 4m \cos\alpha \cot\theta_{xy}(1 - 2c^2)$$

$$- 8 \sin\alpha ac \cot\theta_{xz} M_3 + 4 \sin\alpha (1 - 2c^2)\cot^2\theta_{xy} M_4 - 4 \cos\alpha m^2\cot^2\theta_{xy} M_5$$

$$+ 4 ac \sin\alpha \cot^2\theta_{xz} M_6\Big] \qquad (47)$$

$$C_{m_\alpha} = \frac{L}{3B}(1 - 2 \tan\theta_{xz})C_{N_\alpha} \qquad (48)$$

$$C_{n_\beta} = \frac{L}{3B}(1 - 2 \tan\theta_{xy})C_{Y_\beta} \qquad (49)$$

For the very special case of $\alpha = 0$, $\beta = 0$, these expressions reduce to the following simple expressions

$$C_{N_\alpha} = \frac{L^2}{A(k^2 - 1)} \sin 2\theta_{xz} \tan\theta_{xy}\left[\tan^{-1}\left(\frac{\cot\varphi}{m}\right) - k \tan^{-1}\left(\frac{\cot\varphi}{mk}\right)\right]_{\varphi_1}^{\varphi_2} \qquad (50)$$

$$C_{Y_\beta} = \frac{2L^2}{A} \frac{m \sin\theta_{xz}}{1 - k^2}\left[\frac{1}{k} \tan^{-1}\left(\frac{\cot\varphi}{mk}\right) - \tan^{-1}\left(\frac{\cot\varphi}{m}\right)\right]_{\varphi_1}^{\varphi_2} \qquad (51)$$

The value of C_{l_β} differs in case $m < 1$ or $m > 1$.

For $m < 1$

$$C_{l_\beta} = \left[\frac{4L^3}{3AB}\left(\frac{m^2 - 1}{1 - k^2}\right)\cos\alpha(1 - 2c^2)\tan\theta_{xz}\sin^2\theta_{xz}\right] \times \left[\frac{1}{2m\sqrt{1 - k^2}}\log\left(\frac{\sqrt{\psi} + m\sqrt{1 - k^2}\sin\varphi}{\sqrt{\psi} - m\sqrt{1 - k^2}\sin\varphi}\right) - \frac{\sin\varphi}{\sqrt{\psi}}\right]_{\varphi_1}^{\varphi_2} \tag{52}$$

and for $m > 1$

$$C_{l_\beta} = \left[\frac{4L^3}{3AB}\left(\frac{m^2 - 1}{1 - k^2}\right)\cos\alpha(1 - 2c^2)\tan\theta_{xz}\sin^2\theta_{xz}\right] \times \left[\frac{1}{m\sqrt{k^2 - 1}}\tan^{-1}\left(\frac{m\sqrt{k^2 - 1}\sin\varphi}{\sqrt{\psi}}\right) - \frac{\sin\varphi}{\sqrt{\psi}}\right]_{\varphi_1}^{\varphi_2} \tag{53}$$

The case of $m = 1$ will be discussed in the next section.

C. Special Case of the Circular Cone Segment

The special case of $m = k = 1$ corresponds to the circular cone segments. The previous general expressions can be reduced to the circular cone equations by applying a limiting process as k approaches one. It is to be noted once again that both m and k approach 1 together. The values of these limits are presented in the appendix. Only the final results will be given here.

$$C_N = -\frac{R^2}{A}\left\{a^2 \sin\theta \cos\theta \sin\varphi + ac\cos^2\theta \sin^2\varphi\right.$$

$$- ad\cos^2\theta\left[\varphi + \sin\varphi\cos\varphi\right] + \frac{1}{3}c^2\cot\theta\cos^2\theta\sin^3\varphi$$

$$\left. + \frac{2}{3}dc\cos^2\theta\cot\theta\cos^3\varphi + \frac{1}{3}d^2\cos^2\theta\cot\theta\sin\varphi(\cos^2\varphi + 2)\right|_{\varphi_1}^{\varphi_2}\Bigg\} \quad (54)$$

$$C_A = \frac{R^2}{2A}\left\{2a^2\sin^2\theta - 4ac\sin\theta\cos\theta\cos\varphi - 4ad\sin\theta\cos\theta\sin\varphi\right.$$

$$+ c^2\cos^2\theta(\varphi - \sin\varphi\cos\varphi) - 2cd\cos^2\theta\sin^2\varphi$$

$$\left. + d^2\cos^2\theta(\varphi + \sin\varphi\cos\varphi)\right|_{\varphi_1}^{\varphi_2}\Bigg\} \quad (55)$$

$$C_Y = \frac{R^2}{A}\left\{-a^2\sin\theta\cos\theta\cos\varphi + ac\cos^2\theta(\varphi - \sin\varphi\cos\varphi)\right.$$

$$- ad\cos^2\theta\sin^2\varphi - \frac{1}{3}c^2\cos^2\theta\cot\theta\cos\varphi(\sin^2\varphi + 2)$$

$$\left. - \frac{2}{3}dc\cos^2\theta\cot\theta\sin^3\varphi - \frac{1}{3}d^2\cos^2\theta\cot\theta\cos^3\varphi\right|_{\varphi_1}^{\varphi_2}\Bigg\} \quad (56)$$

$$C_m = \frac{L}{3B} \cot \theta(1 - 2 \tan^2\theta)C_N \tag{57}$$

$$C_n = \frac{L}{3B} \cot \theta(1 - 2 \tan^2\theta)C_Y \tag{58}$$

$$C_l = 0 \tag{59}$$

Equations (20) and (21) with $m = k = 1$ can be used to calculate the value of φ_1 and φ_2. For $m = k = 1$

$$\varphi_1 = \cot^{-1}\left[\frac{-cd \cos^2\theta - a \sin \theta \sqrt{\cos^2\theta - a^2}}{a^2\sin^2\theta - d^2\cos^2\theta}\right] \tag{60}$$

$$\varphi_2 = \cot^{-1}\left[\frac{-cd \cos^2\theta + a \sin \theta \sqrt{\cos^2\theta - a^2}}{a^2\sin^2\theta - d^2\cos^2\theta}\right] \tag{61}$$

It is seen from the above equations that shadow exists if $\cos^2\theta \geq a^2$.

D. Special Cases of $\beta = 0$ and Full and Half Cone Bodies

Relatively simple expressions result for the special case of $\beta = 0$, for both full and half cone bodies. If the reference area is used as the base area, then the expressions for the full cone are: For $m \lessgtr 1$,

and no shadow ($\theta_{xz} \geq \alpha$)

$$C_N = 2 \sin 2\alpha \cos^2\theta_{xz} \tag{62}$$

$$C_A = 2\left[\cos^2\alpha \sin \theta_{xz} \sin \theta_{xy} + \sin^2\alpha \frac{\cos^2\theta_{xz}}{1 + k}\right] \tag{63}$$

These expressions were obtained by using $\beta = 0$, $\varphi_1 = 0$, and $\varphi_2 = 2\pi$ in equations (41) and (42).

Whenever shadow occurs ($\theta_{xz} < \alpha$), C_N and C_A are obtained from equations (41) and (42) with values of φ_1 and φ_2 determined from equations (20) and (21).

The flat top half cone leads to particularly simple results for $\beta = 0$ and $0 \leq \alpha \leq 180 - \theta$. since the curved surface is never shadowed. The proper values of φ_1 and φ_2 to use in equations (41) and (42) are $\varphi_1 = \frac{\pi}{2}$ and $\varphi_2 = \frac{3\pi}{2}$. Then for $m < 1$

$$C_N = -\frac{2}{\pi} \frac{tL}{\left(\frac{t}{2}\right)^2 + L^2} \left[-\frac{\cos^2\alpha}{2\sqrt{1 - k^2}} \log\left(\frac{1 + \sqrt{1 - k^2}}{1 - \sqrt{1 - k^2}}\right) - \frac{\pi L \sin 2\alpha}{t(k + 1)} \right.$$

$$\left. + \frac{4L^2 \sin^2\alpha}{t^2(1 - k^2)} \left(\frac{k^2}{2\sqrt{1 - k^2}} \log \frac{1 + \sqrt{1 - k^2}}{1 - \sqrt{1 - k^2}} - 1 \right) \right] \tag{64}$$

$$C_A = \frac{b^2 k \cos^2\alpha}{2\left[\left(\frac{b}{2}\right)^2 + L^2\right]} + \frac{Lt \sin 2\alpha}{\pi\left[\left(\frac{t}{2}\right)^2 + L^2\right]\sqrt{1 - k^2}} \log\left(\frac{1 + \sqrt{1 - k^2}}{1 - \sqrt{1 - k^2}}\right)$$

$$+ \frac{2L^2 \sin^2\alpha}{\pi\left[\left(\frac{t}{2}\right)^2 + L^2\right](k + 1)} \qquad (65)$$

For $m > 1$

$$C_N = -\frac{2}{\pi} \frac{tL}{\left(\frac{t}{2}\right)^2 + L^2}\left[-\frac{\cos^2\alpha}{\sqrt{k^2 - 1}} \tan^{-1}\sqrt{k^2 - 1} - \frac{\pi L}{t(k + 1)} \sin 2\alpha\right.$$

$$\left. + \frac{4L^2 \sin^2\alpha}{t^2(1 - k^2)}\left(\frac{k^2}{\sqrt{k^2 - 1}} \tan^{-1}\sqrt{k^2 - 1} - 1\right)\right] \qquad (66)$$

$$C_A = \frac{b^2 k \cos^2\alpha}{2\left[\left(\frac{b}{2}\right)^2 + L^2\right]} + \frac{Lt \sin 2\alpha}{\pi\left[\left(\frac{t}{2}\right)^2 + L^2\right]\sqrt{1 - k^2}} \tan^{-1}\sqrt{k^2 - 1} + \frac{2L^2 \sin^2\alpha}{\pi\left[\left(\frac{t}{2}\right)^2 + L^2\right](k + 1)}$$

(67)

For $m = 1$

$$C_N = \frac{2}{\pi}\left[\cos^2\alpha \sin 2\theta + \frac{\pi}{2} \sin 2\alpha \cos^2\theta + \frac{4}{3} \sin^2\alpha \cos^2\theta \cot\theta\right] \qquad (68)$$

$$C_A = 2 \cos^2\alpha \sin^2\theta + \frac{2}{\pi} \sin 2\theta \sin 2\alpha + \sin^2\alpha \cos^2\theta \tag{69}$$

an approximation to the half cone case can be obtained for values of k^2 near unity, for either $k > 1$ or $k < 1$, by expanding the log and $\tan^{-1}$ functions into an infinite series and dropping higher order terms. If $1 - k^2$ is denoted by δ, then

$$\frac{1}{2\sqrt{1 - k^2}} \log \frac{1 + \sqrt{1 - k^2}}{1 - \sqrt{1 - k^2}} = 1 + \frac{1}{3}(1 - k^2) + \frac{1}{5}(1 - k^2)^2 + \ldots$$

$$= 1 + \sum_{n=1}^{\infty} \frac{\delta^n}{2n + 1}$$

$$\frac{1}{\sqrt{k^2 - 1}} \tan^{-1} \sqrt{k^2 - 1} = 1 - \frac{1}{3}(k^2 - 1) + \frac{1}{5}(k^2 - 1)^2 + \ldots$$

$$= 1 + \sum_{n=1}^{\infty} \frac{\delta^n}{2n + 1}$$

Thus for δ small higher ordered terms may be dropped. Then

$$C_N = \frac{2}{\pi} \frac{tL}{\left[\left(\frac{t}{2}\right)^2 + L^2\right]} \left[\cos\alpha \left(1 + \sum_{n=1}^{\infty} \frac{\delta^n}{2n + 1}\right) + \frac{\pi L}{t} \frac{\sin 2\alpha}{k + 1} \right.$$

$$\left. + \frac{4L^2}{t^2} \sin^2\alpha \left(1 - \frac{k^2}{\delta} \sum_{n=1}^{\infty} \frac{\delta^n}{2n + 1}\right)\right] \tag{70}$$

$$C_A = \frac{b^2 k \cos^2\alpha}{2\left[\left(\frac{b}{2}\right)^2 + L^2\right]} + \frac{Lt \sin 2\alpha}{\pi\left[\left(\frac{t}{2}\right)^2 + L^2\right]}\left(1 + \sum_{n=1}^{\infty} \frac{\delta^n}{2n+1}\right)$$

$$+ \frac{2L^2 \sin^2\alpha}{\pi\left[\left(\frac{t}{2}\right)^2 + L^2\right](k+1)} \qquad (71)$$

VII. DISCUSSION

To illustrate the agreement of Newtonian estimates with experimental values, figures 4 through 11 are presented. The experimental results were obtained at Mach numbers of 6.8 and 9.6. The Mach 9.6 data, plotted on figures 5 and 6, were taken from reference 4. The remaining Mach 6.8 and 9.6 data were obtained from reference 8. The theoretical values were obtained from the results of this analysis.

The variation of lift and drag coefficients with angle of attack for a half cone with different fineness ratios or cone half angle, θ_{xz}, and different thickness-to-width ratios, t/b, are shown in figure 4. From this it is seen that, in general, the agreement is good. Both lift and drag coefficients are in excellent agreement with experiment for the lower angle-of-attack range ($\alpha < 25^{\circ}$). At the higher angles of attack, the lift coefficient is predicted with greater accuracy than the drag coefficient. This plot also shows that both coefficients are predicted with greater accuracy for each cone having its major axis, at the base, in the vertical direction (t/b = 2). This might indicate that the "bleeding" of the pressure from the lower to upper surface is not as great when the cone is "tall"as when it is "flat".

Important parameters for most reentry bodies are the maximum values of lift coefficient and lift drag ratio. These parameters are shown plotted for the case of a full circular cone (t/b = 1) against cone half angle, θ, in figure 5. This plot reveals that the maximum lift coefficient is predicted by the theory with a great deal of accuracy for the cone half angles shown. The maximum lift-to-drag ratio is predicted well at the higher cone half angles ($\theta > 20^{\circ}$) but is overpredicted for the more slender cones.

The slopes C_{m_α} and C_{L_α}, for the same full circular cone, are plotted versus cone half angle, θ, in figure 6. Exact inviscid theory was available (ref. 7) for this case and is shown for comparison purposes. It is seen from this figure that there is good agreement between Newtonian theory and the experimental results as well as the exact inviscid theory.

In figure 7, $C_{L,max}$ and $(L/D)_{max}$ for the half cone case are plotted versus the ratio, t/b, for different fineness ratios, t/2L. The variation of $C_{L,max}$ is again predicted quite well. The values of $(L/D)_{max}$, however, are in poor agreement with experiment especially at the lower values of fineness ration ($t/2L < .2$). This poor agreement is due, in part, to the under prediction of the drag coefficients for the more slender bodies.

Figure 8 shows a plot of C_{m_α} and C_{L_α} for the body under consideration versus t/b. The agreement is rather poor for the case of the more slender bodies but improves for the larger values of fineness ratio.

To complete the variation of $C_{L,max}$, $(L/D)_{max}$, C_{m_α}, and C_{L_α} with body parameters, figures 9 and 10 show the variation with body cut-off angle, φ (a value of $\varphi = 90^\circ$ corresponds to a flat-top half cone). Figure 9 shows that both $C_{L,max}$ and $(L/D)_{max}$ are in poor agreement with experiment for the case of the slender 10° cone but improves with increasing cone angle, θ. Figure 10 shows that the slopes, C_{m_α} and C_{L_α} are also in poor agreement for the 10° cone but that the agreement is improved with increasing cone angle.

The lateral derivatives, C_{Y_β} and C_{n_β}, for a half circular cone are plotted versus α in figure 11. Experimental data for C_{l_β} were not

available. Figure 11 indicates that Newtonian theory does a poor job of predicting the side-force derivative, C_{Y_β}, but is in excellent agreement with the yawing moment derivative, C_{n_β}, for both cone half angles. The value of C_{l_β} (C_l taken about the center line) is predicted to be zero for this case. For the case of the elliptical cone, however, C_{l_β} as well as the other derivatives are all dependent on the body parameters, m, k, and the body cut-off angle φ.

VIII. CONCLUSIONS

Newtonian theory was applied, in this analysis, to the elliptic cone segment at angles of attack and sideslip. Closed form expressions for the aerodynamic coefficients and static stability derivatives were obtained. Expressions for the full and half conic bodies were given and approximate expression in powers of $1 - k^2$ were given for the half cone case. The circular cone results were obtained as a special case of the general results.

Comparisons of the theoretical calculation with experimental results indicate that this theory provides an invaluable tool in obtaining first approximations to the aerodynamic characteristics of segments of circular and elliptical cones in the hypersonic flow regime. Tabulated values from these expressions for various values of t/b, $t/2L$, and φ through the angle-of-attack range of 0° to 90° and values of β from 0° to 15° would be of great benefit to anyone with need of a quick approximation to the aerodynamic characteristics of these particular bodies. Such tabulated values will be available in the form of a NASA technical note by the author which is to be published at a later date.

Comparisons of the theory with experiment indicate that the Newtonian results are, in general, in very good agreement with experiment for the blunter cones at the smaller angles of attack ($\alpha < 25^\circ$ and blunter $\theta > 20^\circ$ or $t/2L > 0.3$). All coefficients except $(L/D)_{max}$ and C_{Y_β} were predicted with very good accuracy. For higher values of α the agreement was good only for the blunter cones ($t/2L > 0.3$). Predictions of $(L/D)_{max}$ and C_{Y_β} were the least successful of all cases shown. Comparisons with Newtonian theory such as these are presented in more detail in references 4 and 8. These references indicate the above agreement between experiment and theory is typical for conic body shapes.

IX. ACKNOWLEDGMENTS

The author wishes to express his appreciation to the National Aeronautics and Space Administration for the opportunity to use material in this thesis which was obtained from a research project conducted at their Langley Center.

He also wishes to thank Dr. Hassan A. Hassan and Dr. Robert W. Truitt of the Aeronautical Engineering Department of the Virginia Polytechnic Institute, and of the Aero-Physics Division of NASA for their advice and assistance in preparing this thesis.

X. BIBLIOGRAPHY

1. Grimminger, G., Williams, E. P., and Young, G. B. W.: Lift on Inclined Bodies of Revolution in Hypersonic Flow. Jour. Aero. Sci., vol. 17, no. 11, November 1950, pp. 675-690.

2. Seaman, Donna J., and Dore, Frank J.: Force and Pressure Coefficients of Elliptic Cones and Cylinders in Newtonian Flow. Consolidated Vultee Report ZA-7-004. May 16, 1952.

3. Truitt, Robert W.: Hypersonic Aerodynamics. The Ronald Press Company. New York, 1959.

4. Penland, J. A.: Aerodynamic Force Characteristics of a Series of Lifting Cone and Cone-Cylinder Missile Configurations at Mach Number 6.83 and Angles of Attack up to 90°. NASA TN D-840.

5. Armstrong, William O.: Aerodynamic Characteristics of Several Series of Lifting Bodies Applicable to Reentry Vehicle Design. NASA TM X-536.

6. Amick, James L.: Pressure Measurements on Sharp and Blunt 5° and 15° Half-Angle Cones at Mach Number 3.86 and Angles of Attack to 100°. NASA TN D-753, 1961.

7. Ames Research Staff: Equations, Tables, and Charts for Compressible Flow. NACA TR 1135. 1953.

8. Wells, W. R., and Armstrong, W. O.: Tables of Aerodynamic Coefficients Obtained From Developed Newtonian Expressions for Full and Partial Conic and Spheric Body Segments at Combined Angles of Attack and Sideslip Along With Some Comparisons With Hypersonic Experimental Data. Prospective NASA TN.

The vita has been removed from the scanned document

XII. APPENDIX

The values of the integrals $I_1, I_2, \ldots I_5, I_6$ are tabulated below:

$$I_1 = \int \frac{\cos\varphi\, d\varphi}{\Omega\sqrt{\psi}} = \frac{1}{m\sqrt{k^2-1}} \tan^{-1}\left(\frac{m\sqrt{k^2-1}\sin\varphi}{\sqrt{\psi}}\right) + C, \quad k > 1$$

$$= \frac{1}{2m\sqrt{1-k^2}} \log\left(\frac{\sqrt{\psi} + m\sqrt{1-k^2}\sin\varphi}{\sqrt{\psi} - m\sqrt{1-k^2}\sin\varphi}\right) + C, \quad k < 1$$

$$I_2 = \int \frac{\sin\varphi\cos\varphi\, d\varphi}{\Omega\psi} = \frac{1}{2m^2(k^2-1)} \log\frac{\Omega}{\psi} + C$$

$$I_3 = \int \frac{\cos\varphi\, d\varphi}{\Omega\psi} = \frac{1}{m(k^2-1)}\left[\tan^{-1}\left(\frac{\cot\varphi}{m}\right) - k\tan^{-1}\left(\frac{\cot\varphi}{mk}\right)\right] + C$$

$0 < \varphi < \pi, \quad \pi < \varphi < 2\pi$

$$I_4 = \int \frac{\sin\varphi\cos^2\varphi\, d\varphi}{\Omega\psi^{3/2}} = \frac{1}{m^2(1-k^2)}\left[\frac{k}{\sqrt{1-k^2}} \tan^{-1}\left(\frac{\cos\varphi\sqrt{1-k^2}}{k\sqrt{\psi}}\right) - \frac{\cos\varphi}{\psi}\right] + C, \quad k < 1$$

$$I_4 = \frac{1}{m^2(1-k^2)}\left[\frac{k}{2\sqrt{k^2-1}}\log\left(\frac{\sqrt{\psi}+\frac{\cos\varphi}{k}\sqrt{k^2-1}}{\sqrt{\psi}-\frac{\cos\varphi}{k}\sqrt{k^2-1}}\right)-\frac{\cos\varphi}{\sqrt{\psi}}\right]+C,\ k>1$$

$$I_5 = \int\frac{\cos\varphi\sin^2\varphi\,d\varphi}{\Omega_\psi^{3/2}} = \frac{1}{m^2(1-k^2)}\left[\frac{1}{m\sqrt{k^2-1}}\tan^{-1}\left(\frac{m\sqrt{k^2-1}\sin\varphi}{\sqrt{\psi}}\right)\right.$$

$$\left.-\frac{\cos\varphi}{\sqrt{\psi}}\right]+C,\quad k>1$$

$$I_5 = \frac{1}{m^2(1-k^2)}\left[\frac{1}{2m\sqrt{1-k^2}}\log\left(\frac{\sqrt{\psi}+m\sqrt{1-k^2}\sin\varphi}{\sqrt{\psi}-m\sqrt{1-k^2}\sin\varphi}\right)-\frac{\sin\varphi}{\sqrt{\psi}}\right]+C,\quad k<1$$

$$I_6 = \int\frac{\cos\varphi\,d\varphi}{\Omega_\psi^{3/2}} = \frac{1}{1-k^2}\left[\frac{-k^2}{2m\sqrt{1-k^2}}\log\left(\frac{\sqrt{\psi}+m\sqrt{1-k^2}\sin\varphi}{\sqrt{\psi}-m\sqrt{1-k^2}\sin\varphi}\right)\right.$$

$$\left.+\frac{\sin\varphi}{\sqrt{\psi}}\right]+C,\ k<1$$

$$I_6 = \frac{1}{1-k^2}\left[\frac{-k^2}{m\sqrt{k^2-1}}\tan^{-1}\left(\frac{m\sqrt{k^2-1}\sin\varphi}{\sqrt{\psi}}\right)+\frac{\sin\varphi}{\sqrt{\psi}}\right]+C,\quad k>1$$

$$J_1 = \int \frac{d\varphi}{\Omega} = -\frac{1}{mk} \tan^{-1}\left(\frac{\cot \varphi}{mk}\right) 0 < \varphi < \pi, \quad \pi < \varphi < 2\pi$$

$$J_2 = \int \frac{\sin \varphi \, d\varphi}{\Omega \sqrt{\psi}} = -\frac{1}{mk \sqrt{1 - k^2}} \tan^{-1}\left(\frac{\cos \varphi \sqrt{1 - k^2}}{k \sqrt{\psi}}\right) + C, \; k < 1$$

$$J_2 = -\frac{1}{2m^2 k \sqrt{k^2 - 1}} \log\left(\frac{\sqrt{\psi} + \frac{\cos \varphi}{k} \sqrt{k^2 - 1}}{\sqrt{\psi} - \frac{\cos \varphi}{k} \sqrt{k^2 - 1}}\right) + C, \; k > 1$$

$$J_3 = \int \frac{\cos \varphi \, d\varphi}{\Omega \sqrt{\psi}} = \frac{1}{m \sqrt{k^2 - 1}} \tan^{-1}\left(\frac{m \sqrt{k^2 - 1} \sin \varphi}{\sqrt{\psi}}\right) + C, \; k > 1$$

$$J_3 = \frac{1}{2m \sqrt{1 - k^2}} \log\left(\frac{\sqrt{\psi} + m \sqrt{1 - k^2} \sin \varphi}{\sqrt{\psi} - m \sqrt{1 - k^2} \sin \varphi}\right) + C, \; k < 1$$

$$J_4 = \int \frac{\cos \varphi \sin \varphi \, d\varphi}{\Omega \psi} = I_2$$

$$J_5 = \int \frac{\sin^2 \varphi \, d\varphi}{\Omega \psi} = \frac{1}{m^3 (k^2 - 1)} \left[\frac{1}{k} \tan^{-1}\left(\frac{\cot \varphi}{mk}\right) - \tan^{-1}\left(\frac{\cot \varphi}{m}\right)\right] + C$$

$0 < \varphi < \pi, \quad \pi < \varphi < 2\pi$

$$J_6 = \int \frac{\cos \varphi \, d\varphi}{\Omega\psi} = I_3$$

$$L_1 = J_2$$

$$L_2 = J_5$$

$$L_3 = I_2$$

$$L_4 = I_5$$

$$L_5 = \int \frac{\sin \varphi \, d\varphi}{\Omega\psi^{3/2}} = \frac{1}{m^4(k^2 - 1)}\left[\frac{1}{k\sqrt{1 - k^2}} \tan^{-1} \frac{\cos \varphi\sqrt{1 - k^2}}{k\sqrt{\psi}} - \frac{\cos \varphi}{\sqrt{\psi}}\right] + C,$$

$k < 1$

$$L_5 = \frac{1}{m^4(k^2 - 1)}\left[\frac{1}{2k\sqrt{k^2 - 1}} \log\left(\frac{\sqrt{\psi} + \frac{\cos \varphi}{k}\sqrt{k^2 - 1}}{\sqrt{\psi} - \frac{\cos \varphi}{k}\sqrt{k^2 - 1}}\right) - \frac{\cos \varphi}{\sqrt{\psi}}\right] + C, \quad k > 1$$

$$L_6 = I_4$$

$$M_1 = I_2$$

$$M_2 = I_5$$

$$M_3 = I_4$$

$$M_4 = \int \frac{\sin\varphi\cos\varphi\,d\varphi}{\Omega\psi^2} = \frac{1}{2m^2(k^2-1)}\left[\frac{\sin\varphi\cos\varphi}{\psi} + \frac{1}{m}\tan^{-1}\left(\frac{\cot\varphi}{m}\right)\right]$$

$$+ \frac{k^2}{m^3(1-k^2)^2}\left[\frac{1}{k}\tan^{-1}\left(\frac{\cot\varphi}{mk}\right) - \tan^{-1}\left(\frac{\cot\varphi}{m}\right)\right] + C,\quad 0 < \varphi < \pi,\quad \pi < \varphi < 2\pi$$

$$M_5 = \int \frac{\sin\varphi\cos\varphi\,d\varphi}{\Omega\psi} = -\frac{1}{2m^2(k^2-1)}\left[\frac{1}{m^2(k^2-1)}\log\frac{\Omega}{\psi} + \frac{1}{m^2-1}\frac{1}{\psi}\right] + C$$

$$M_6 = \int \frac{\cos^3\varphi\,\sin\varphi\,d\varphi}{\Omega\psi^2} = \frac{1}{2(k^2-1)}\left[\frac{k^2}{m^2(k^2-1)}\log\frac{\Omega}{\psi} + \frac{1}{m^2-1}\frac{1}{\psi}\right] + C$$

In the limiting case of $m,\ k = 1$ it is necessary to take the limit of each term of the coefficients as $m,\ k$ approaches unity. These are shown below:

$$\lim_{\substack{k\to 1\\ m\to 1}} \frac{1}{\sqrt{1-k^2}}\log\left(\frac{\sqrt{\psi} + m\sqrt{1-k^2}\sin\varphi}{\sqrt{\psi} - m\sqrt{1-k^2}\sin\varphi}\right) = 2\sin\varphi$$

$$\lim_{\substack{k\to 1\\ m\to 1}} \frac{1}{k^2-1}\log\frac{\Omega}{\psi} = \sin\varphi$$

$$\lim_{\substack{k \to 1 \\ m \to 1}} \frac{1}{k^2 - 1}\left[\tan^{-1}\left(\frac{\cot \varphi}{m}\right) - k \tan^{-1}\left(\frac{\cot \varphi}{mk}\right)\right] = \frac{1}{2}\left(\varphi - \frac{\pi}{2} + \sin \varphi \cos \varphi\right)$$

$$\lim_{\substack{k \to 1 \\ m \to 1}} \frac{1}{k^2 - 1}\left[\frac{k}{\sqrt{1 - k^2}} \tan^{-1}\left(\frac{\sqrt{1 - k^2}\cos \varphi}{k\sqrt{\psi}}\right) - \frac{\cos \varphi}{\sqrt{\psi}}\right] = -\frac{1}{3} \cos \varphi$$

$$\lim_{\substack{k \to 1 \\ m \to 1}} \frac{1}{1 - k^2}\left[\frac{1}{2m\sqrt{1 - k^2}} \log\left(\frac{\sqrt{\psi} + m\sqrt{1 - k^2}\sin \varphi}{\sqrt{\psi} - m\sqrt{1 - k^2}\sin \varphi}\right) - \frac{\sin \varphi}{\sqrt{\psi}}\right] = \frac{1}{3} \sin^3 \varphi$$

$$\lim_{\substack{k \to 1 \\ m \to 1}} \frac{1}{1 - k^2}\left[\frac{-k^2}{2m\sqrt{1 - k^2}} \log\left(\frac{\sqrt{\psi} + m\sqrt{1 - k^2}\sin \varphi}{\sqrt{\psi} - m\sqrt{1 - k^2}\sin \varphi}\right) + \frac{\sin \varphi}{\sqrt{\psi}}\right] = \frac{1}{3} \sin \varphi(\cos^2 \varphi + 2)$$

$$\lim_{\substack{k \to 1 \\ m \to 1}} \frac{1}{\sqrt{k^2 - 1}} \tan^{-1}\left(\frac{m\sqrt{k^2 - 1}\sin \varphi}{\sqrt{\psi}}\right) = \sin \varphi$$

$$\lim_{\substack{k \to 1 \\ m \to 1}} \frac{1}{1 - k^2}\left[\frac{k}{2\sqrt{k^2 - 1}} \log\left(\frac{\sqrt{\psi} + \frac{\sqrt{k^2 - 1}}{k}\cos \varphi}{\sqrt{\psi} - \frac{\sqrt{k^2 - 1}}{k}\cos \varphi}\right) - \frac{\cos \varphi}{\sqrt{\psi}}\right] = -\frac{1}{3} \cos^3 \varphi$$

$$\lim_{\substack{k \to 1 \\ m \to 1}} \frac{1}{1 - k^2}\left[\frac{1}{m\sqrt{k^2 - 1}} \tan^{-1}\left(\frac{m\sqrt{k^2 - 1}\sin \varphi}{\sqrt{\psi}}\right) - \frac{\sin \varphi}{\sqrt{\psi}}\right] = \frac{1}{3} \sin^3 \varphi$$

$$\lim_{\substack{k \to 1 \\ m \to 1}} \frac{1}{1 - k^2}\left[\frac{-k^2}{m\sqrt{k^2 - 1}} \tan^{-1}\left(\frac{m\sqrt{k^2 - 1}\sin \varphi}{\sqrt{\psi}}\right) + \frac{\sin \varphi}{\sqrt{\psi}}\right] = \frac{1}{3} \sin \varphi(\cos^2 \varphi + 2)$$

$$\lim_{\substack{k \to 1 \\ m \to 1}} \frac{1}{mk} \tan^{-1}\left(\frac{\cot \varphi}{mk}\right) = \frac{\pi}{2} - \varphi$$

$$\lim_{\substack{k \to 1 \\ m \to 1}} \frac{1}{\sqrt{1 - k^2}} \tan^{-1}\left(\frac{\sqrt{1 - k^2}}{k} \frac{\cos \varphi}{\sqrt{\psi}}\right) = \cos \varphi$$

$$\lim_{\substack{k \to 1 \\ m \to 1}} \frac{1}{k^2 - 1}\left[\frac{1}{k} \tan^{-1}\left(\frac{\cot \varphi}{mk}\right) - \tan^{-1}\left(\frac{\cot \varphi}{m}\right)\right] = \frac{1}{2}(\varphi - \frac{\pi}{2} - \sin \varphi \cos \varphi)$$

$$\lim_{\substack{k \to 1 \\ m \to 1}} \frac{1}{\sqrt{k^2 - 1}} \log\left(\frac{\sqrt{\psi} + \frac{\sqrt{k^2 - 1}}{k} \cos \varphi}{\sqrt{\psi} - \frac{\sqrt{k^2 - 1}}{k} \cos \varphi}\right) = 2 \cos \varphi$$

$$\lim_{\substack{k \to 1 \\ m \to 1}} \frac{1}{k^2 - 1}\left[\frac{1}{k\sqrt{1 - k^2}} \tan^{-1}\left(\frac{\sqrt{1 - k^2}}{k} \frac{\cos \varphi}{\sqrt{\psi}}\right) - \frac{\cos \varphi}{\sqrt{\psi}}\right] = \frac{1}{3} \cos \varphi(\sin \varphi + 2)$$

$$\lim_{\substack{k \to 1 \\ m \to 1}} \frac{1}{k^2 - 1}\left[\frac{1}{2k\sqrt{k^2 - 1}} \log\left(\frac{\sqrt{\psi} + \frac{\sqrt{k^2 - 1}}{k} \cos \varphi}{\sqrt{\psi} - \frac{\sqrt{k^2 - 1}}{k} \cos \varphi}\right) - \frac{\cos \varphi}{\sqrt{\psi}}\right] =$$

$$- \frac{2}{3} \cos \varphi(\sin^2 \varphi + 2)$$

In the case of C_l, the presence of the term $(m^2 - 1)$ multiplied out front causes the entire expression to be zero when $k \to 1$ and $m \to 1$. Thus $\lim_{\substack{k \to 1 \\ m \to 1}} C_l = 0$.

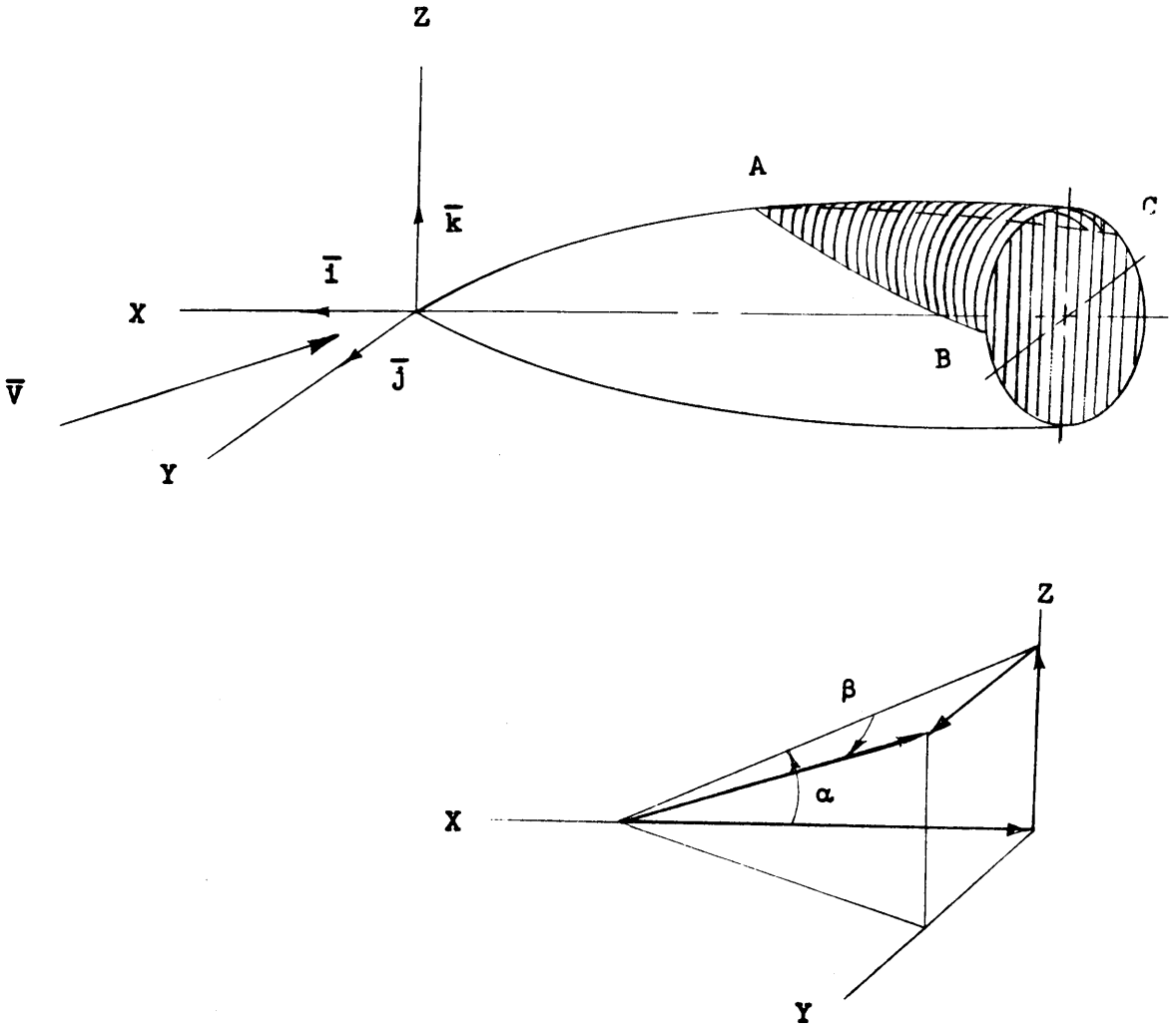

Figure 1.- General body coordinate system and wind components.

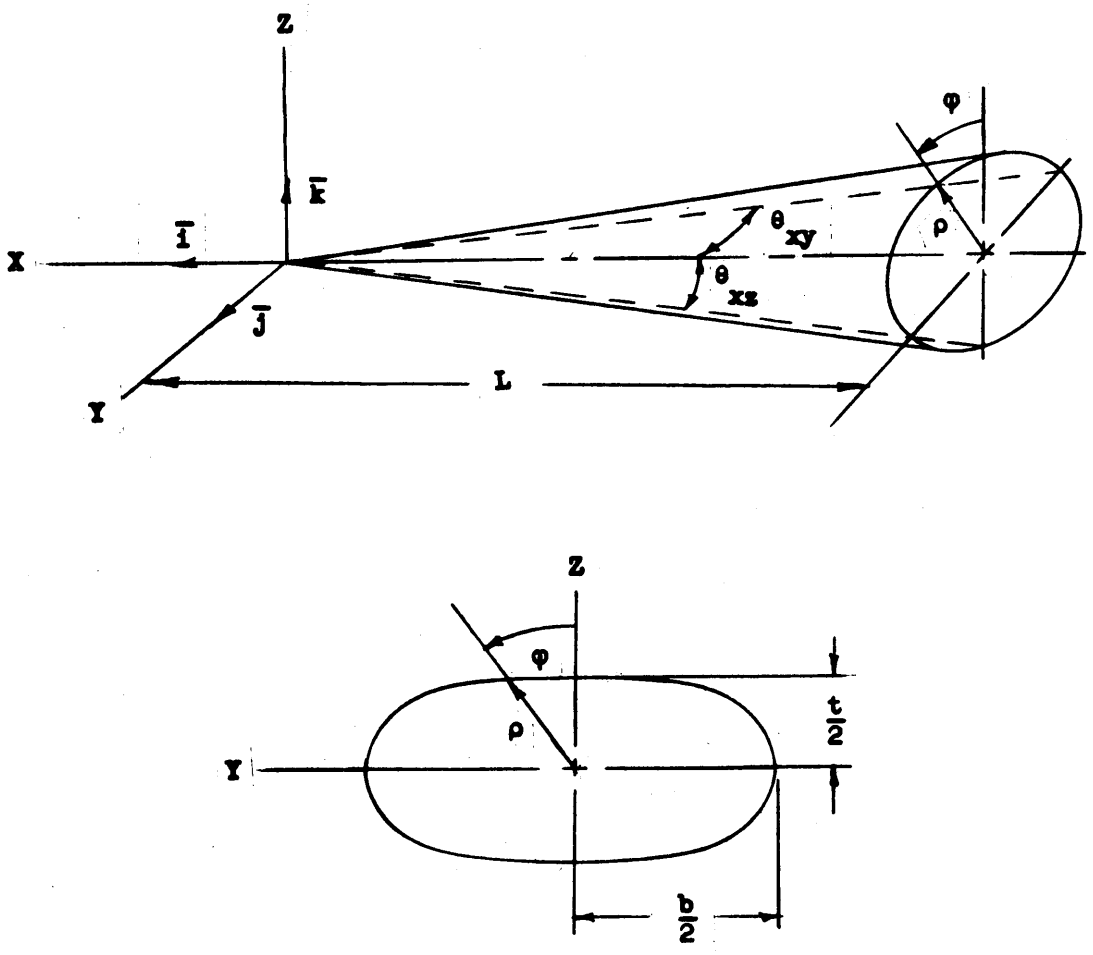

Figure 2.- Coordinate system and characteristic lengths and angles for elliptical cone body.

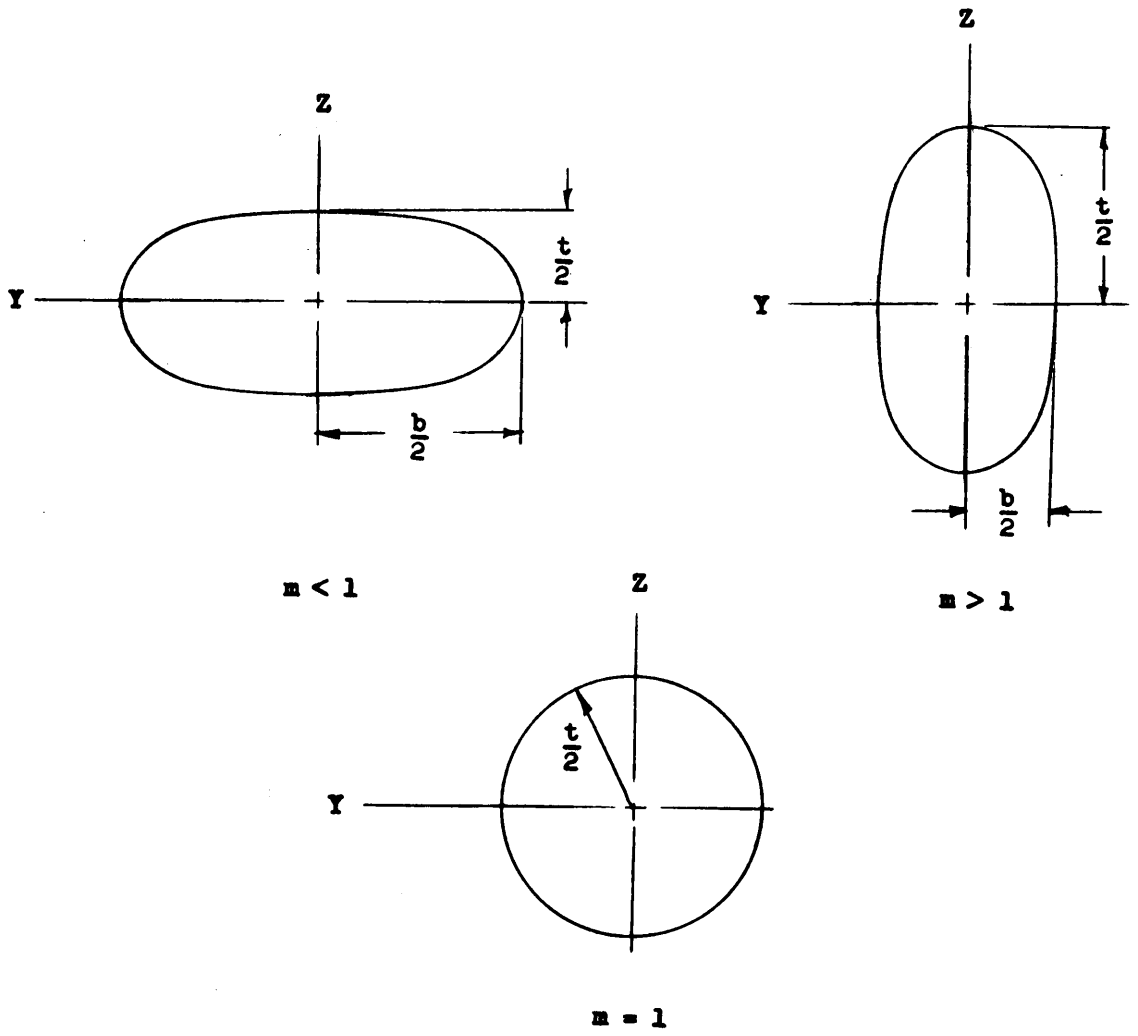

Figure 3.- Cross-sectional views at station X = -L for cases of m < 1, m = 1, and m > 1.

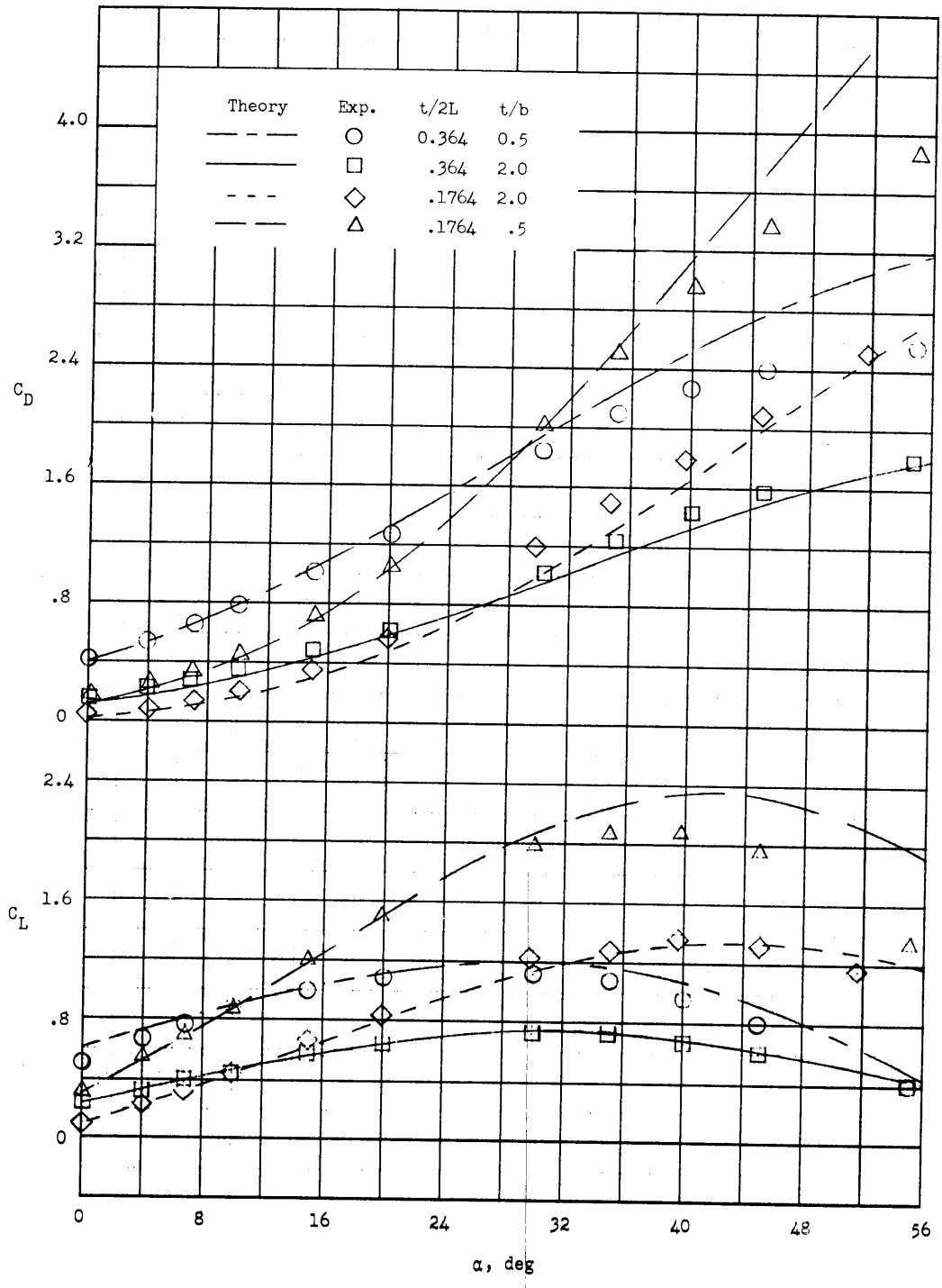

Figure 4.- Variation of lift and drag coefficients with angle of attack for half cone at $\beta = 0$. Experimental data obtained at $M = 9.6$.

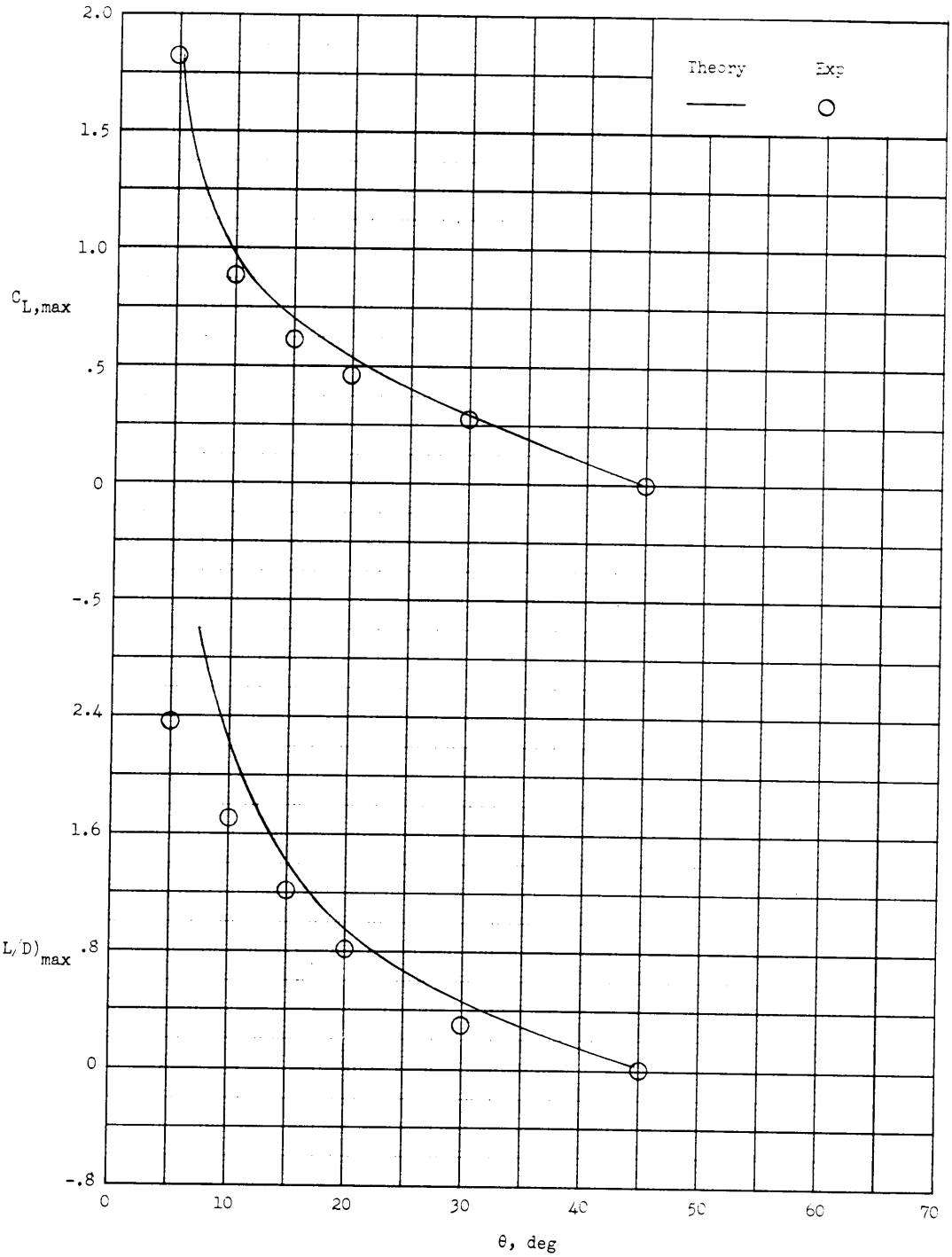

Figure 5.- Variation of $C_{L,max}$ and $(L/D)_{max}$ with cone semiapex angle for full cone with $t/b = 1$. Experimental values obtained at $M = 6.8$.

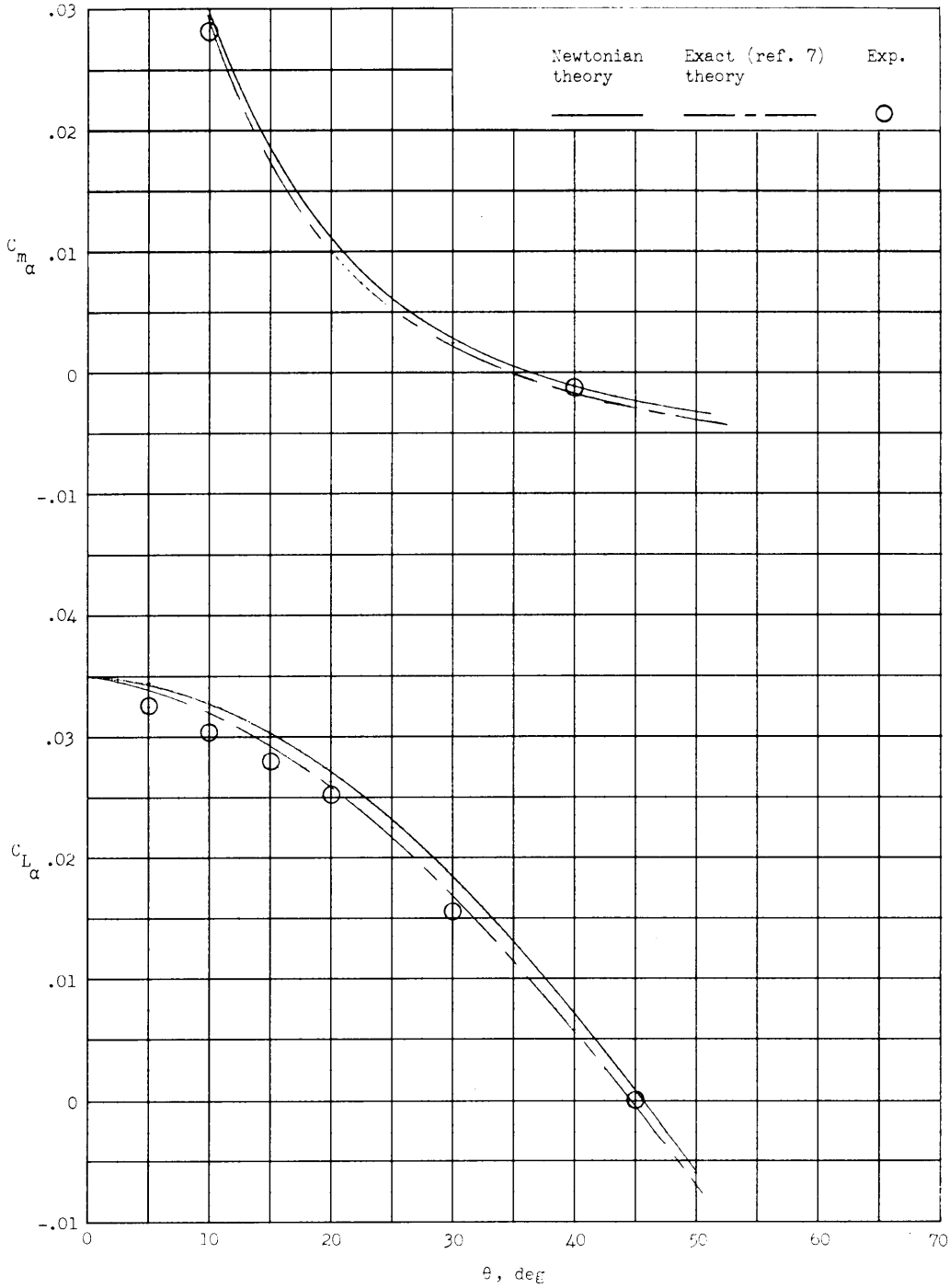

Figure 6.- Variation of lift and moment slopes with cone semiapex angle for full cone with t/b = 1. Experimental values obtained at M = 6.8.

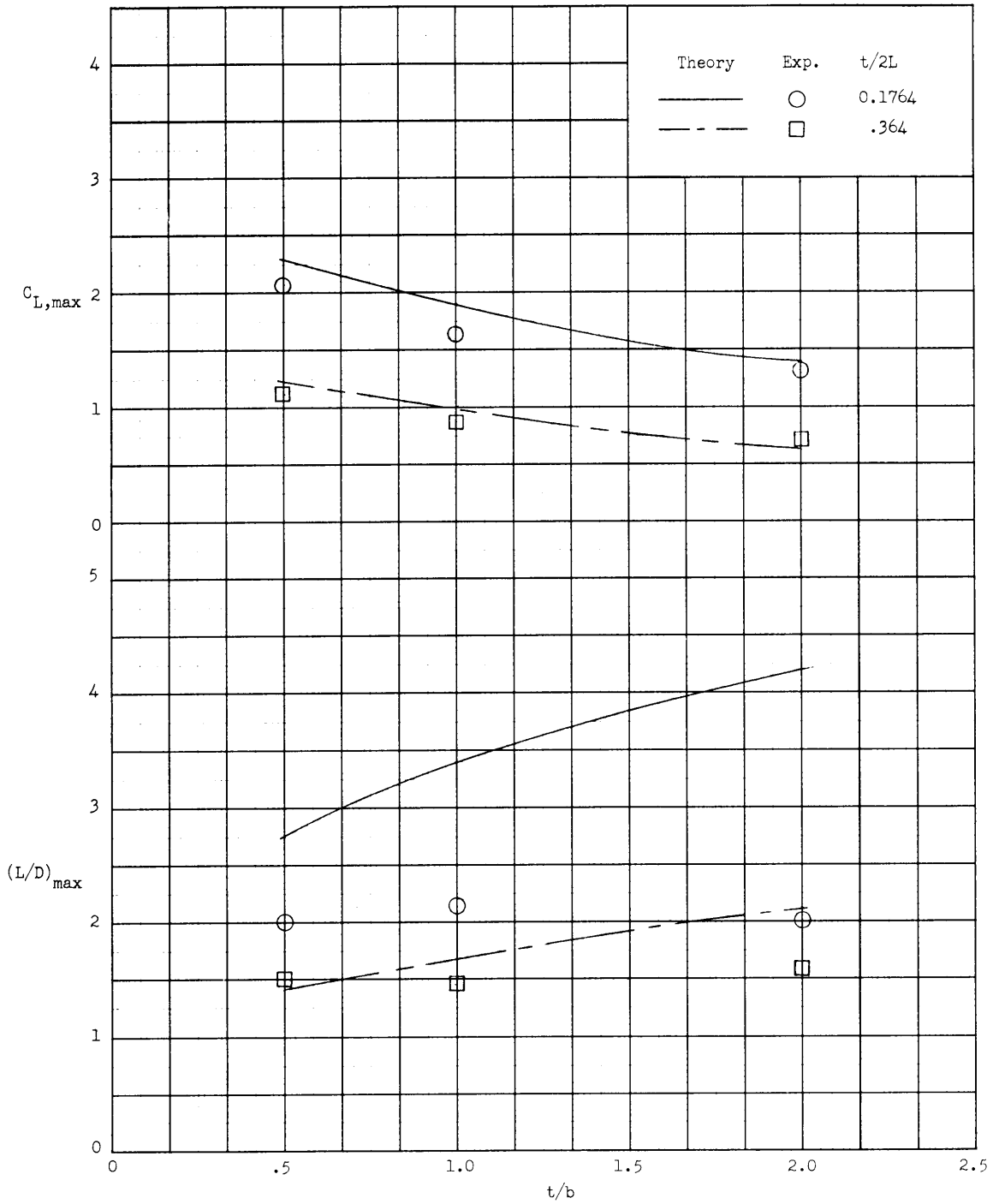

Figure 7.- Variation of $C_{L,max}$ and $(L/D)_{max}$ with thickness ratio for half cone bodies. Experimental values obtained at M = 9.6.

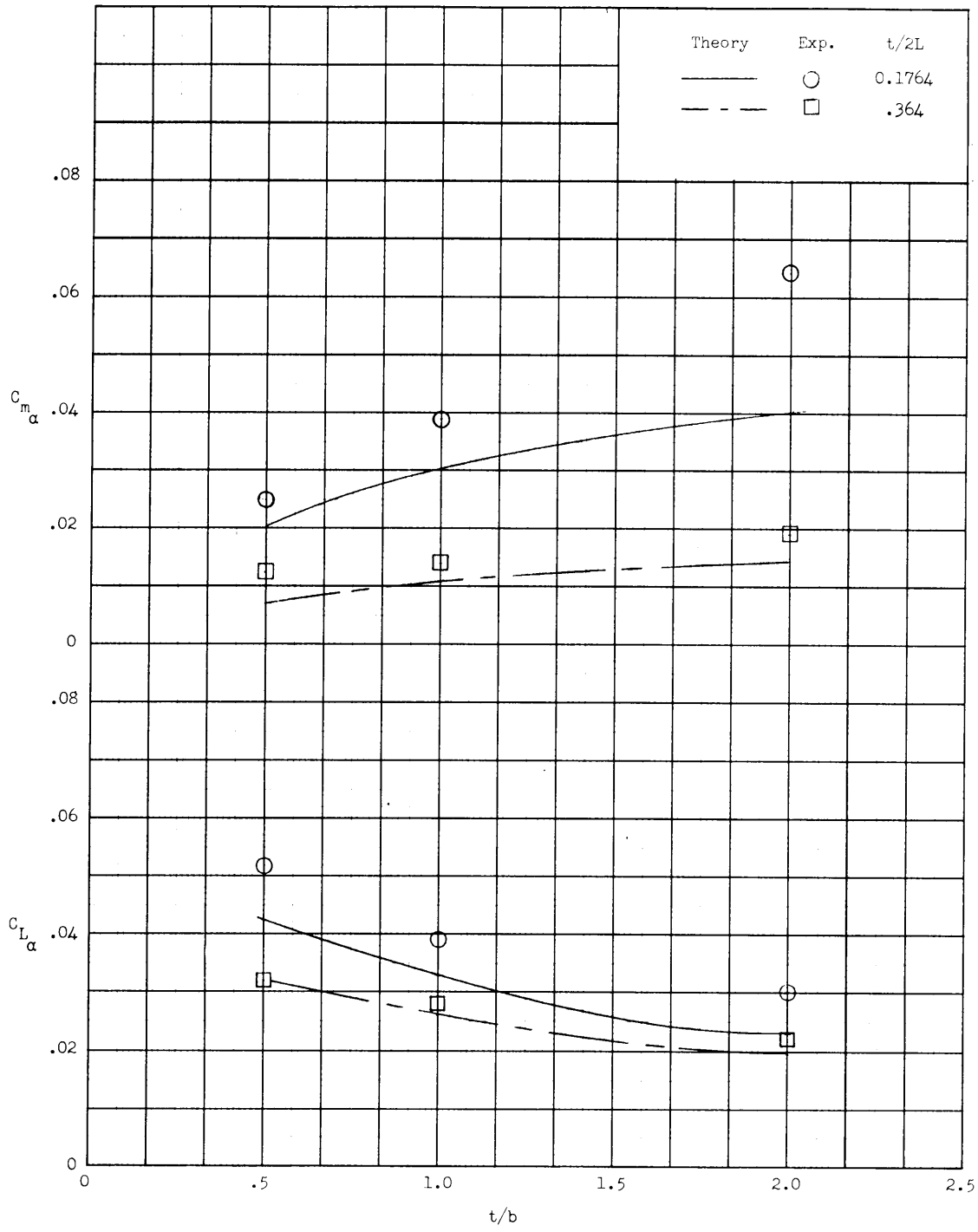

Figure 8.- Variation of lift and moment slopes with cone thickness ratio for half cone bodies at $\beta = 0$. Experimental values obtained at $M = 9.6$.

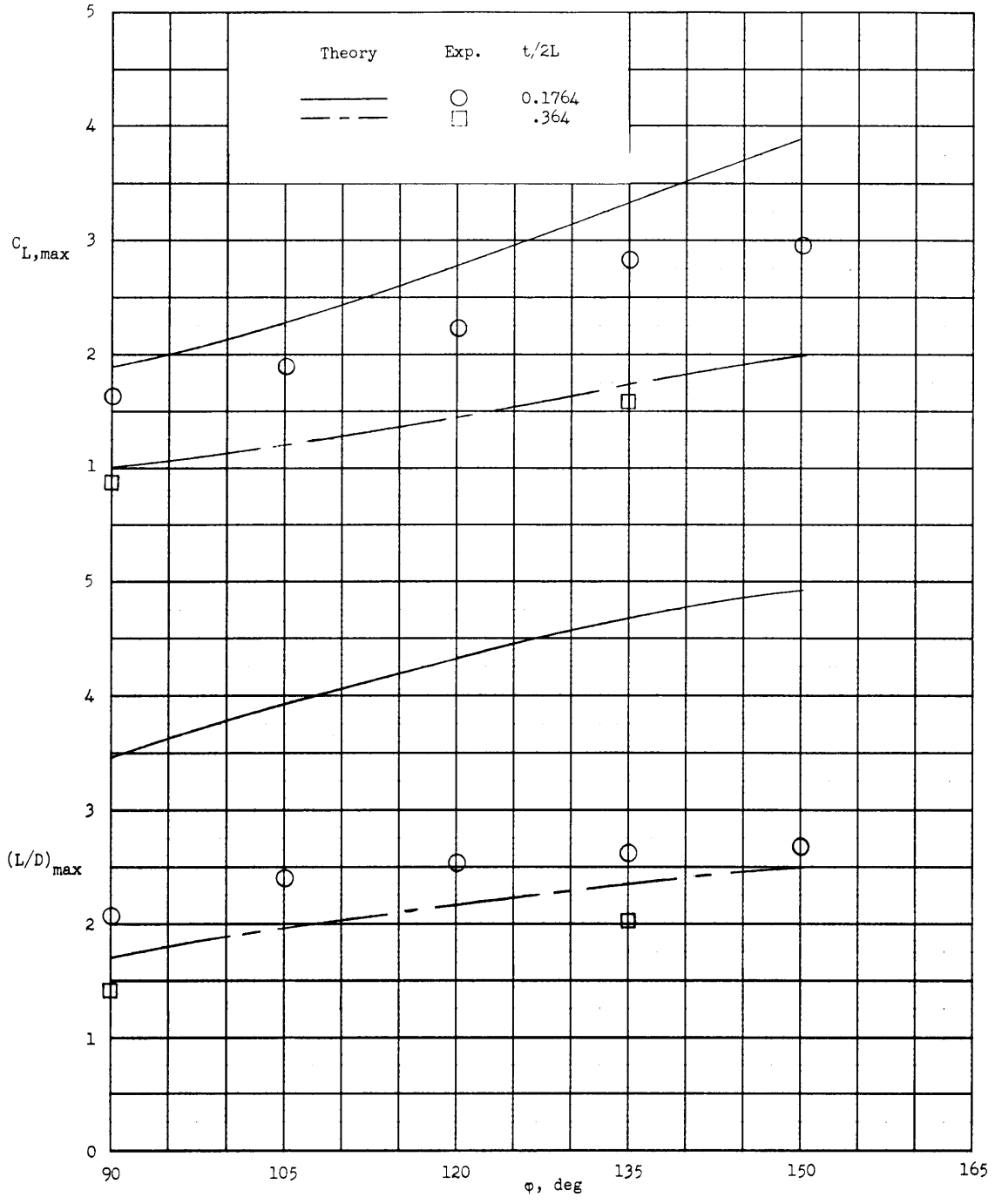

Figure 9.- Variation of $C_{L,max}$ and $(L/D)_{max}$ with body segment for different cone semiapex angles with $t/b = 1$. Experimental values obtained at $M = 9.6$.

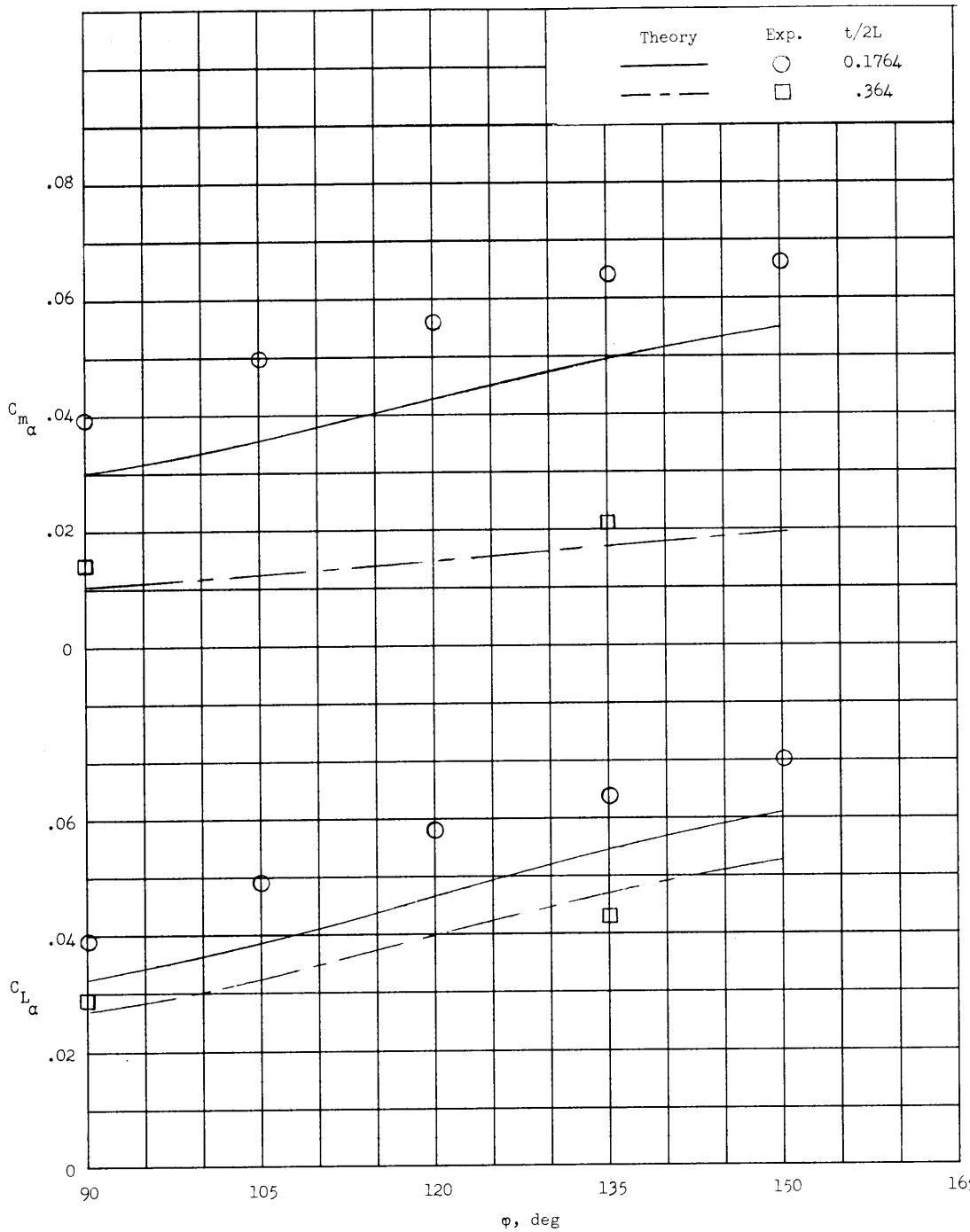

Figure 10.- Variation of lift and moment slopes with body segment for different cone semiapex angles at $\beta = 0$ and $t/b = 1$. Experimental values obtained at $M = 9.6$.

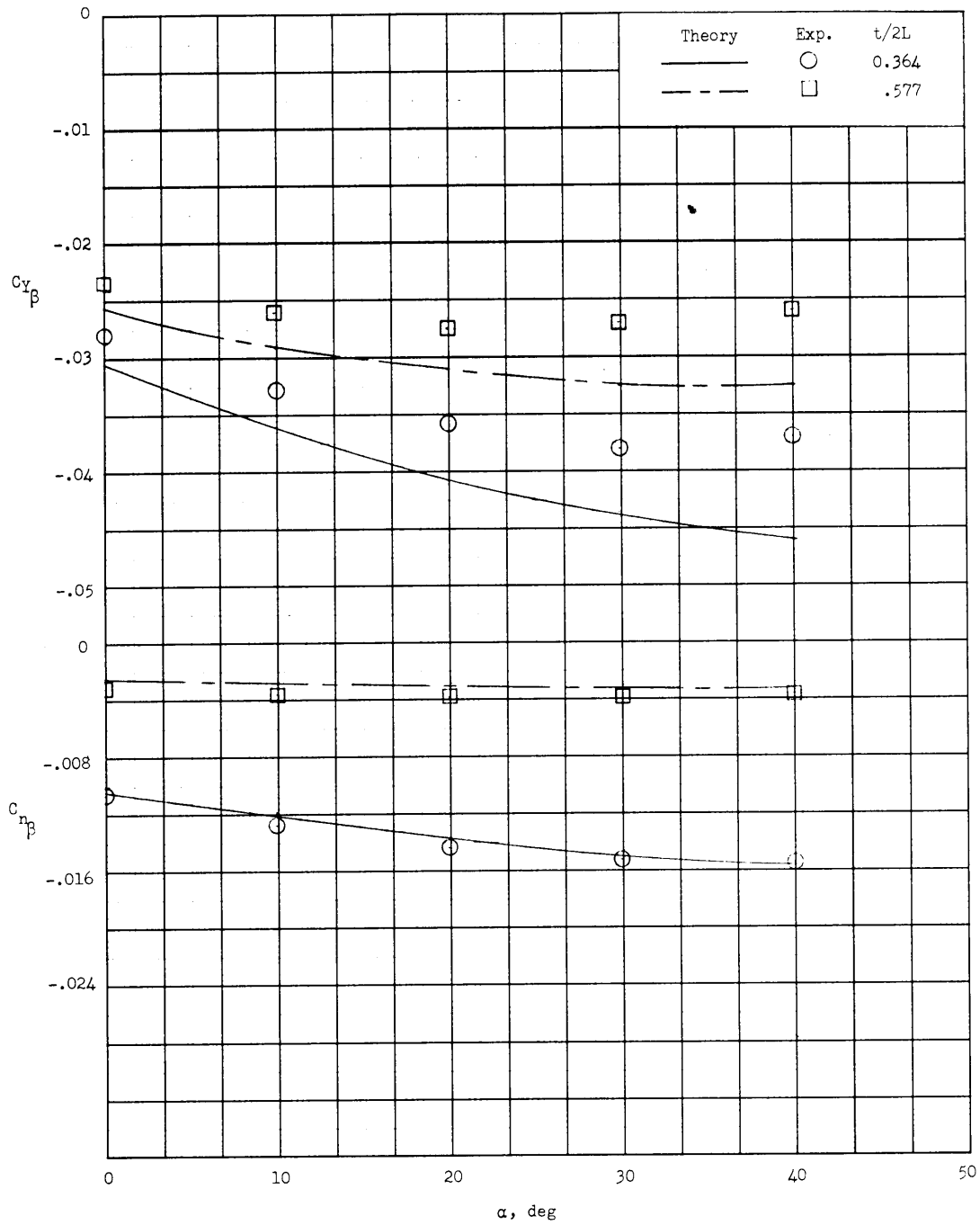

Figure 11.- Variation of the slopes, C_{Y_β} and C_{n_β} with angle of attack for half cone with $t/b = 1$. Experimental values obtained at $M = 6.8$.

THE PREDICTION OF AERODYNAMIC FORCE AND MOMENT COEFFICIENTS ON ELLIPTIC CONE BODIES AT BOTH ANGLE OF ATTACK AND SIDESLIP BY USE OF NEWTONIAN IMPACT THEORY

by

William R. Wells

ABSTRACT

Newtonian theory was applied, in this analysis, to the elliptic cone segment at angles of attack and sideslip. Closed form expressions for the aerodynamic coefficients and static stability derivatives were obtained. Expressions for the full and half conic bodies were given and approximate expressions were given for the half cone case. The circular cone results were obtained as a special case of the general results.

Comparisons of the theoretical calculations with experimental results at hypersonic speeds were made of the aerodynamic coefficients and static derivatives for several conic segments. Generally, good agreement was observed for specified ranges of fineness ratios and angles of attack.